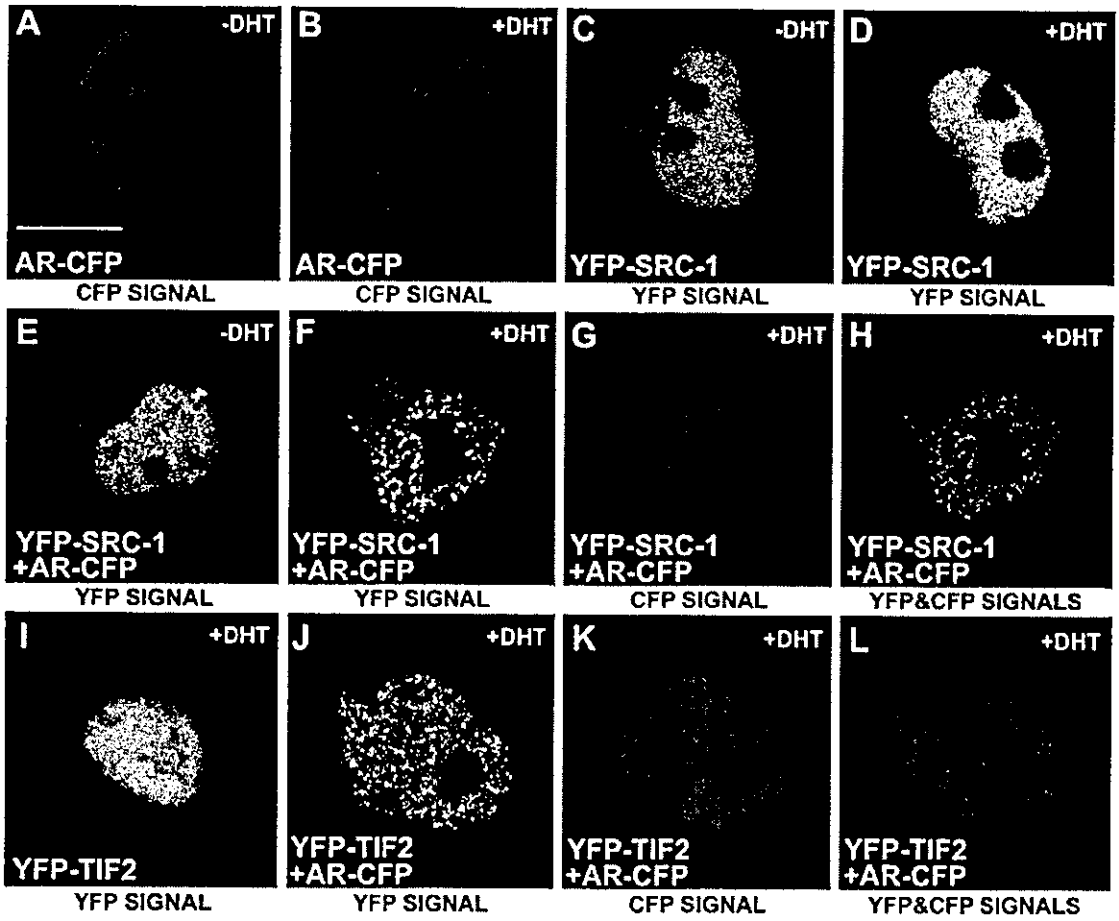

Fig. 1. Subcellular Localization of AR-CFP, YFP-SRC-1, and YFP-TIF2 in COS7 Cells

COS7 cells were transfected with the expression plasmids for AR-CFP (0.5 μg) (A and B), YFP-SRC-1 (0.5 μg) (C and D), YFP-TIF2 (0.5 μg) (I), or YFP-SRC-1 (0.3 μg) (E–H) or YFP-TIF2 (0.3 μg) (J–L) in addition to AR-CFP (0.25 μg), and the expressed chimeric fluorescent proteins were observed in living cells by confocal laser scanning microscopy as described in *Materials and Methods*. E–H and J–L, The transfected amounts of pCMV-YFP-SRC-1, -YFP-TIF2, and -AR-CFP were equivalent on a molar basis. The treatment or absence of treatment with 10^{-8} M 5α-DHT, the expression plasmid transfected, and the fluorescent signal observed are indicated *in or just below each panel*. The fluorescent signals from CFP and YFP are represented as *red* and *yellow*, respectively, by digital color conversion on a computer. *Bar*, 10 μm.

observations suggest that CBPΔ (118–2393) exerted its dominant negative effect by occupying a CBP-binding site of the AR but not by binding to a trans-activation complex to which endogenous CBP binds. This explanation for the dominant negative effect of CBPΔ (118–2393) is not inconsistent because the N-terminal 100 amino acid residues of CBP have been reported to contain a domain for nuclear receptor binding (12).

Subnuclear Distribution and Transcriptional Activation Function of the N-Terminal and C-Terminal AR Fragments Fused to Fluorescent Protein

AR-AF-1-YFP, in which YFP was fused to the C terminus of the AR-AF-1 fragment, consisting of the AF-1-containing NTD and the DNA-binding domain (DBD) of the AR, was distributed in a foci-forming pattern in the nucleus of COS7 cells regardless of the presence of DHT (Fig. 4, A and B). In contrast, AR-AF-2-CFP, in which CFP was fused to the C terminus of the AR-AF-2 fragment, consisting of the DBD and the AF-2-containing ligand-binding domain (LBD) of the AR, was distributed in a uniform pattern regardless of the presence of DHT (Fig. 4, G and H). The subnuclear distribution pattern was similar in the AR fragments in which fluorescent protein was fused to the N termini of the AR fragments (data not shown). When, in addition to pCMV-AR-AF-1-YFP, pCMV-AR-AF-2-CFP was cotransfected at an amount lower than that of pCMV-AR-AF-1-YFP on a molar basis, the foci formation of AR-AF-1-YFP collapsed (Fig. 4C). Cotransfection of

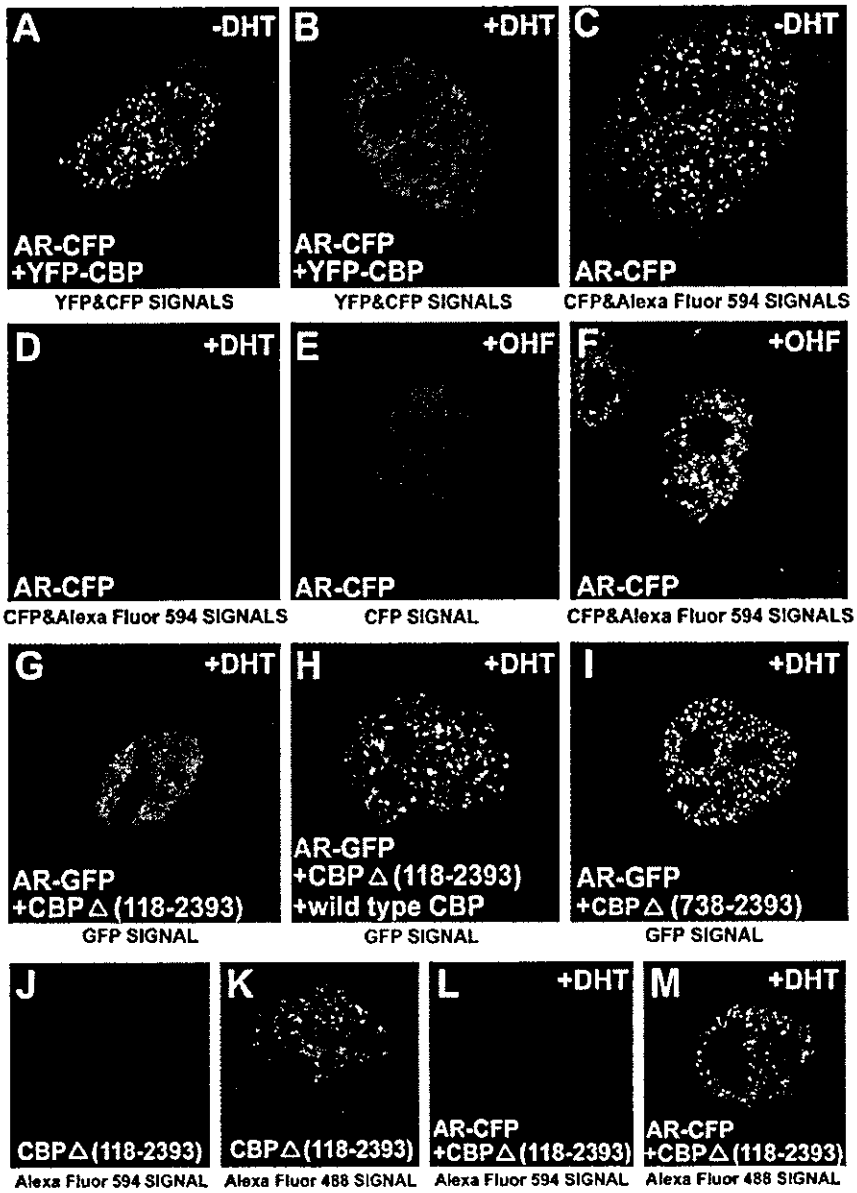

Fig. 2. Subcellular Distribution of AR-CFP and YFP-CBP, and Effect of the Truncated CBP on the Subnuclear Localization of AR-GFP in COS7 Cells

COS7 cells were transfected with the expression vectors for AR-CFP alone (0.15 μg) (C–F), YFP-CBP (0.35 μg) plus AR-CFP (0.15 μg) (A and B), CBPΔ (118–2393) (1.0 μg) alone (J and K), AR-GFP (0.15 μg) in combination with CBPΔ (118–2393) (1.0 μg) (G), CBPΔ (118–2393) (1.0 μg) plus wild-type CBP (0.2 μg) (H), or CBPΔ (738–2393) (1.5 μg) (I), or AR-CFP (0.15 μg) in combination with CBPΔ (118–2393) (1.0 μg) (L and M). The molar equivalents of the transfected amount of the plasmids for AR-CFP, YFP-CBP, AR-GFP, CBPΔ (118–2393), wild-type CBP, and CBPΔ (738–2393) were 1, 1, 1, 48, 0.7, and 15, respectively. The treatment or absence of treatment with 10^{-8} M DHT or 10^{-6} M OHF, the expression plasmid transfected and the fluorescent signal observed are indicated *in or just below each panel*. CFP (A–F) and GFP (G–I) signals are represented as *red* and *green*, respectively. The YFP signal from YFP-CBP (A and B) and the Alexa Fluor 594 signal due to immunostaining of endogenous CBP (C, D, and F) are represented as *yellow*. The Alexa Fluor 488 signal due to immunostaining of only endogenous CBP (K and M) is represented as *green*. The Alexa Fluor 594 signal due to immunostaining of both CBPΔ (118–2393) and endogenous CBP (J and L) is represented as red. Primary anti-CBP antibodies used were CBP (451) in J and L and CBP (C-1) in K and M. In C, D, and F, CBP(A-22) was used in addition to CBP (451) and CBP (C-1), and essentially the same results were obtained. Panels J and L show a diffusely stained pattern, reflecting overexpressed CBPΔ (118–2393), although endogenous CBP was also stained.

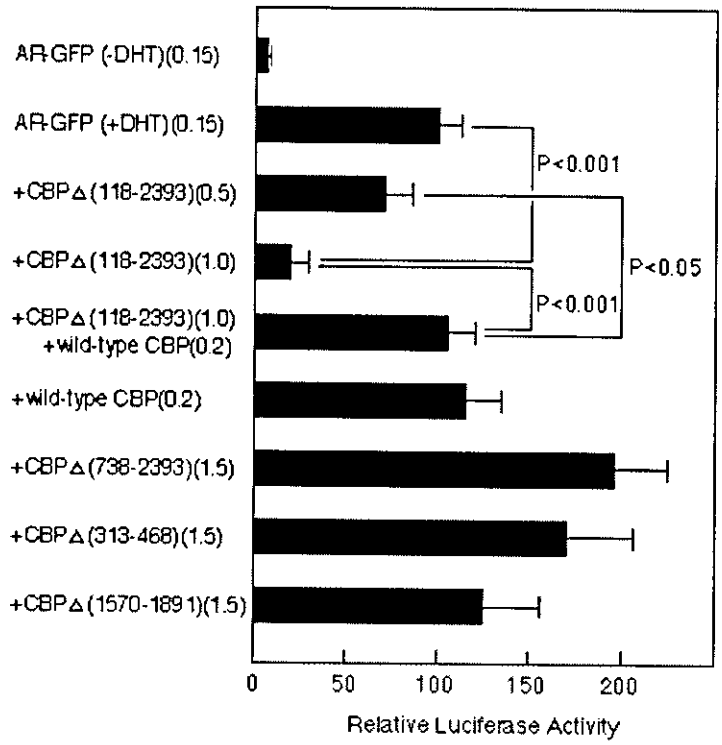

Fig. 3. Repression of AR-Dependent Transactivation by CBPΔ (118–2393) and Its Reversal by Coexpressed Wild-Type CBP

COS7 cells were transfected with the indicated amounts (μg) of the expression vectors for AR-GFP and the truncated or wild-type CBP, along with the reporter genes, as described in *Materials and Methods*. The luciferase activities are represented as values relative to the activity induced by AR-GFP alone in the presence of 10^{-8} M DHT, which was arbitrarily set as 100. Each *bar* represents the mean ± SD of three independent experiments.

pCMV-AR-AF-2-CFP at an amount higher than that of pCMV-AR-AF-1-YFP perfectly excluded AR-AF-1-YFP from the nucleus to the cytosol (Fig. 4D). However, AR-AF-1-YFP was translocated again into the nucleus with foci formation by the addition of DHT (Fig. 4E), and AR-AF-2-CFP was also distributed with foci formation coinciding with AR-AF-1-YFP (Fig. 4F). Both the AR-AF-1-YFP and AR-AF-2-CFP fragments contained the DBD. Therefore, there was a possibility that the overlapped DBDs affected the interaction between AR-AF-1 and AR-AF-2. The DBD-deleted NTD, Δ(DBD)AR-AF-1-YFP, was distributed dominantly in the cytosol (Fig. 4I), probably because this fragment lacked the nuclear localization signal (NLS). Δ(DBD)AR-AF-1-YFP was translocated into the nucleus with foci formation in the presence of DHT-bound AR-AF-2-CFP (Fig. 4J) as seen in cells transfected with both pCMV-AR-AF-1-YFP and pCMV-AR-AF-2-CFP (Fig. 4, E and F), indicating that the overlapped DBD did not hinder the function of each AR fragment. When pCMV-YFP-SRC-1 or pCMV-YFP-TIF2 was cotransfected with pCMV-AR-AF-1-CFP, these coactivators formed foci coinciding with AR-AF-1-CFP (Fig. 4, K and L). AR-AF-1-YFP activated the transcription of the luciferase reporter gene regardless of the presence of DHT, and the level of the transactivation function was about 70% of that of the AR-AF-1 not fused to YFP. Although AR-AF-2-CFP showed ligand-dependent transcription activation, it was less than 6% of that of AR-AF-1-YFP (Fig. 5). Ligand-independent transactivation by AR-AF-1-YFP was suppressed to about 17% of the original activity by cotransfection of equivalent amounts or twice as much of pCMV-AR-AF-2-CFP in the absence of DHT, but transactivation increased 3 to 4 times in the presence of DHT (Fig. 5). Essentially similar results were obtained with the AR fragments, which were not fused to fluorescent protein (Fig. 5) and in the experiments using CV-1 and LNCaP cells (data not shown).

Construction of the Three-Dimensional Image of the Subnuclear Distribution of the N-Terminal and C-Terminal AR Fragments Fused to Fluorescent Protein

Although foci formation in the nucleus was closely correlated with the presence of transactivation function in not only the full-length AR but also the AR fragments (Figs. 1–5), the existence of foci formation did not reflect differences in the levels of the transcriptional activation function. The formation of foci was evenly observed by two-dimensional imaging among cells transfected with the expression vectors for the

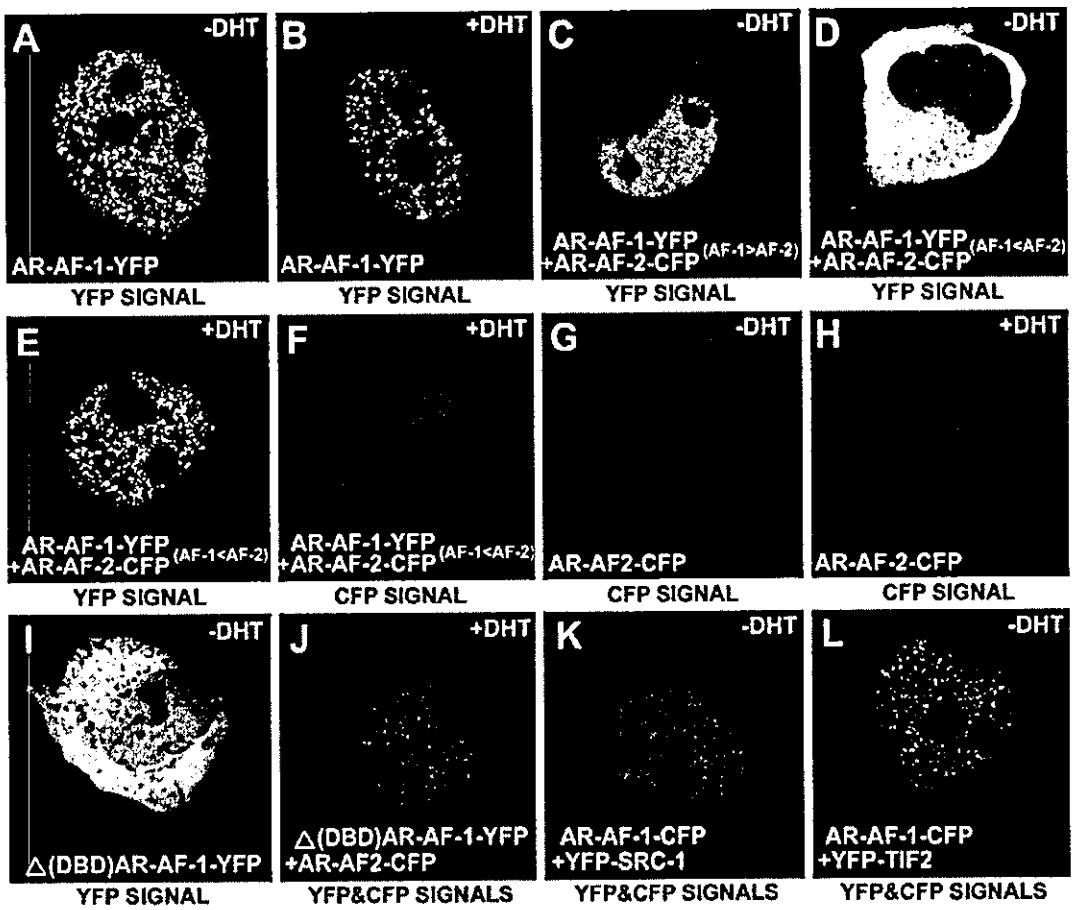

Fig. 4. Subcellular Distribution of the N-Terminal (AR-AF-1) and C-Terminal (AR-AF-2) Fragments Tagged with Fluorescent Proteins

COS7 cells were transfected with the expression plasmids indicated in each panel, and then the living cells were scanned. The transfected amount of the plasmid was 0.5 μg in panels A, B, G, and H. The molar ratios of the transfected amounts of pCMV-AR-AF-1-YFP and pCMV-AR-AF-2-CFP were 2:1 (0.35 and 0.15 μg, respectively) in C and 1:2 (0.18 and 0.32 μg, respectively) in D–F. I–L, Transfected amounts of the expression plasmids for Δ(DBD)AR-AF-1-YFP (0.2 μg), AR-AF-2-CFP (0.19 μg), YFP-SRC-1 (0.28 μg), YFP-TIF2 (0.28 μg), and AR-AF-1-CFP (0.22 μg) were equivalent on a molar basis. The addition of 10^{-8} M DHT and the fluorescent signal observed are indicated *in or just below each panel.* The CFP and YFP signals are represented as *red* and *yellow*, respectively.

full-length AR-CFP, the AR-AF-1-YFP alone and the AR-AF-1-YFP in combination with the AR-AF-2-CFP (Figs. 1B and 4, B and E), although the levels of transactivation were different (Fig. 5). Therefore, to clarify whether any differences in the subnuclear localization exist among these AR fragments and the full-length AR, we analyzed the intranuclear distribution by a computer-assisted three-dimensional imaging method. Nuclear DNA in living cells was stained with Hoechst 33342, which has been used to discriminate the heterochromatin region from the euchromatin region. To obtain the heterochromatin image, the less stained areas (namely euchromatin region) were cut off and shown as blank images (Fig. 6E). Most of the liganded full-length AR-GFP was detected as discrete multiple spots (Fig. 6A, surface view), and the green spots were located in the euchromatin region (Fig. 6F, surface view). In contrast, AR-AF-2-CFP was homogenously distributed as a single large spot, except for the nucleoli, regardless of the presence of DHT (Fig. 6C, surface view), over the whole chromatin (Fig. 6, I, surface view, and J, tomographic view). AR-AF-1-YFP was distributed in an intermediate pattern between the patterns of the full-length AR and the AR-AF-2-CFP, *i.e.* a reticular pattern (Fig. 6B, surface), in which the spatial distribution of the YFP signal was not discontinuous and was calculated as one volume, mostly in the euchromatin region (Fig. 6, G, surface, and H, tomogram). However, in combination with DHT-bound AR-AF-2-CFP, the AR-AF-1-YFP formed isolated spots and showed distribution which was essentially identical with that of the full-length AR-GFP (Fig. 6, D,

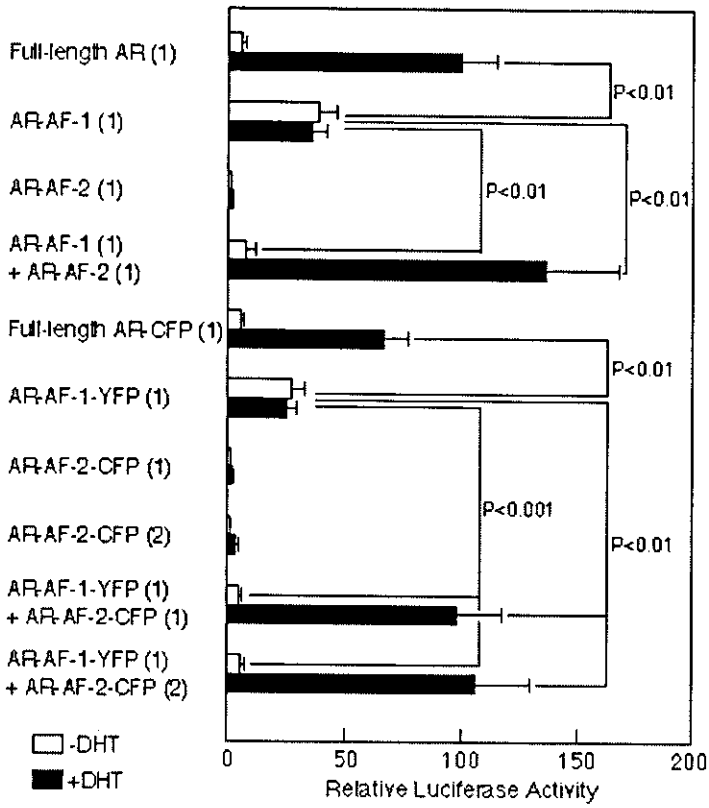

Fig. 5. Transcriptional Activation by Full-Length AR, the Truncated ARs, and Their Chimeras with Fluorescent Proteins in COS7 Cells

COS7 cells were transfected with the expression vectors for full-length AR (0.2 μg), the N-terminal fragment (AR-AF-1) (0.18 μg), the C-terminal fragment (AR-AF-2) (0.16 μg), and their chimeras with fluorescent proteins as indicated, along with the reporter genes, as described in *Materials and Methods*. The numbers in *parentheses* indicate the molar equivalents of the vectors transfected by setting that of the full-length AR as 1.0. The luciferase activities are represented as values relative to the activity induced by full-length AR alone in the presence of 10^{-8} M DHT, which was arbitrarily set as 100. Each *bar* represents the mean ± SD of three independent experiments.

surface, and K, tomogram). The DHT-bound AR-AF-2-CFP in combination with the DBD-deleted NTD, Δ(DBD)AR-AF-1, also formed isolated spots (Fig. 6L, surface), indicating that overlapped DBDs of the AR-AF-1 and AR-AF-2 fragments did not affect the interaction between the two fragments. Essentially the same results were obtained using CV-1 and LNCaP cells.

Quantitative Analysis of Intranuclear Foci of the AR, GR, and ERα by Three-Dimensional Imaging

The present three-dimensional construction method for the confocal images, in which a rejection of scattering fluorescence with a low degree of brightness and median filter processing were carried out, allowed us to observe intranuclear fluorescent proteins at a high resolution and to quantify the number of fluorescent spots in the nucleus. Approximately 300 AR-CFP spots (see legend for Fig. 7) were found to exist as a distinct volume in one nucleus (Fig. 7A). The nuclear volume occupied by these 300 spots was estimated to be approximately 10% of the total nuclear volume in the present experimental conditions. When the three-dimensional imaging method was applied to liganded GR-YFP and ERα-GFP, in which YFP and GFP were fused to the C termini of GR and ERα, respectively, a distribution of discrete spots in the nucleus was also observed (Fig. 7, B and C), and the numbers of spots (308 ± 23, n = 8) were similar to that of AR-CFP. The number of spots was calculated from the three-dimensional images processed under the same conditions. When pCMV-AR-CFP was cotransfected with pCMV-GR-YFP, they formed identical spots in the presence of their ligands (Fig. 7D), and naturally the number of spots was similar to that of AR-CFP or GR-YFP alone. Similar results were obtained by the cotransfection of AR-CFP and ERα-GFP (Fig. 7E). The number of AR-CFP spots was not affected by cotransfection, *i.e.* overexpression, of coactivators such as YFP-SRC-1, YFP-TIF2 and YFP-CBP (see legend for Fig. 7). Fur-

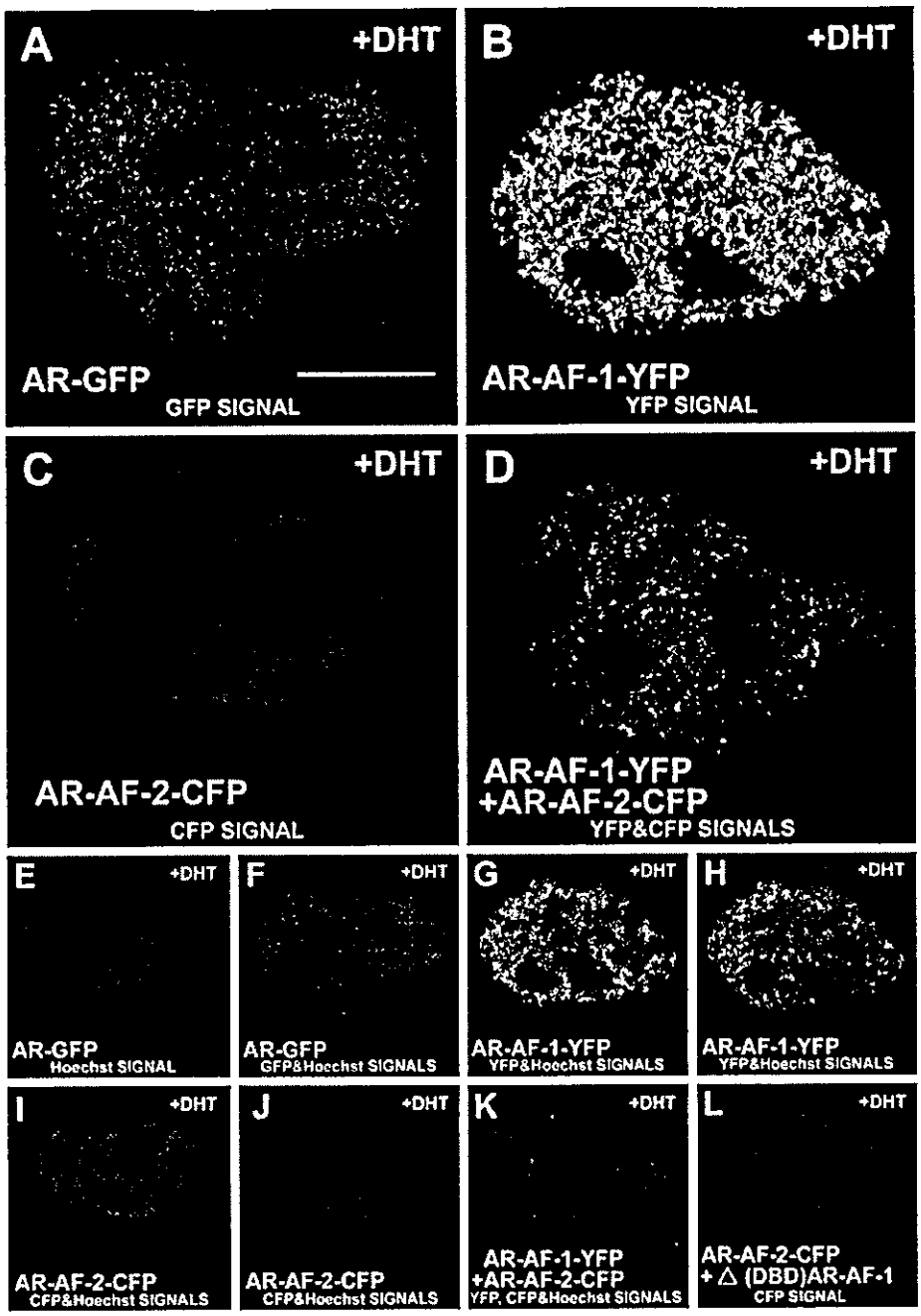

Fig. 6. The Three-Dimensional Image Analysis of the Intranuclear Localization of the N-Terminal (AR-AF-1) and C-Terminal (AR-AF-2) AR Fragments Tagged with Fluorescent Proteins in COS7 Cells

COS7 cells transfected with the expression plasmids were treated with 10^{-8} M DHT and stained with Hoechst 33342. Next, the confocal images of the nuclei in living cells were collected to reconstruct the three-dimensional images. The expression plasmids transfected are indicated in each panel. In panel A, 0.25 μg of pCMV-AR-GFP was transfected, and the amounts of each plasmid transfected in other panels were equivalent on a molar basis. The images were displayed as a surface view (A–G, I and L) or a tomographic sectional view on the z-axis (H, J, and K). The fluorescent signals from GFP, YFP, CFP, and Hoechst 33342 are represented as *green*, *yellow*, *red*, and *blue*, respectively. A, AR-GFP foci formation in the nucleus; B, reticular distribution of AR-AF-1-YFP; C, diffuse and homogenous distribution of AR-AF-2-CFP; D, *orange*-colored foci formation by AR-AF-1-YFP and AR-AF-2-CFP; E, chromatin structure stained with Hoechst 33342; F, spatially superimposed three-dimensional image of A and E; G and H, superimposed image of B and the chromatin structure; I and J, superimposed image of C and the chromatin structure; K, superimposed image of D and the chromatin structure; L, foci formation by Δ(DBD)AR-AF-1 and AR-AF-2-CFP. *Bar*, 5 μm.

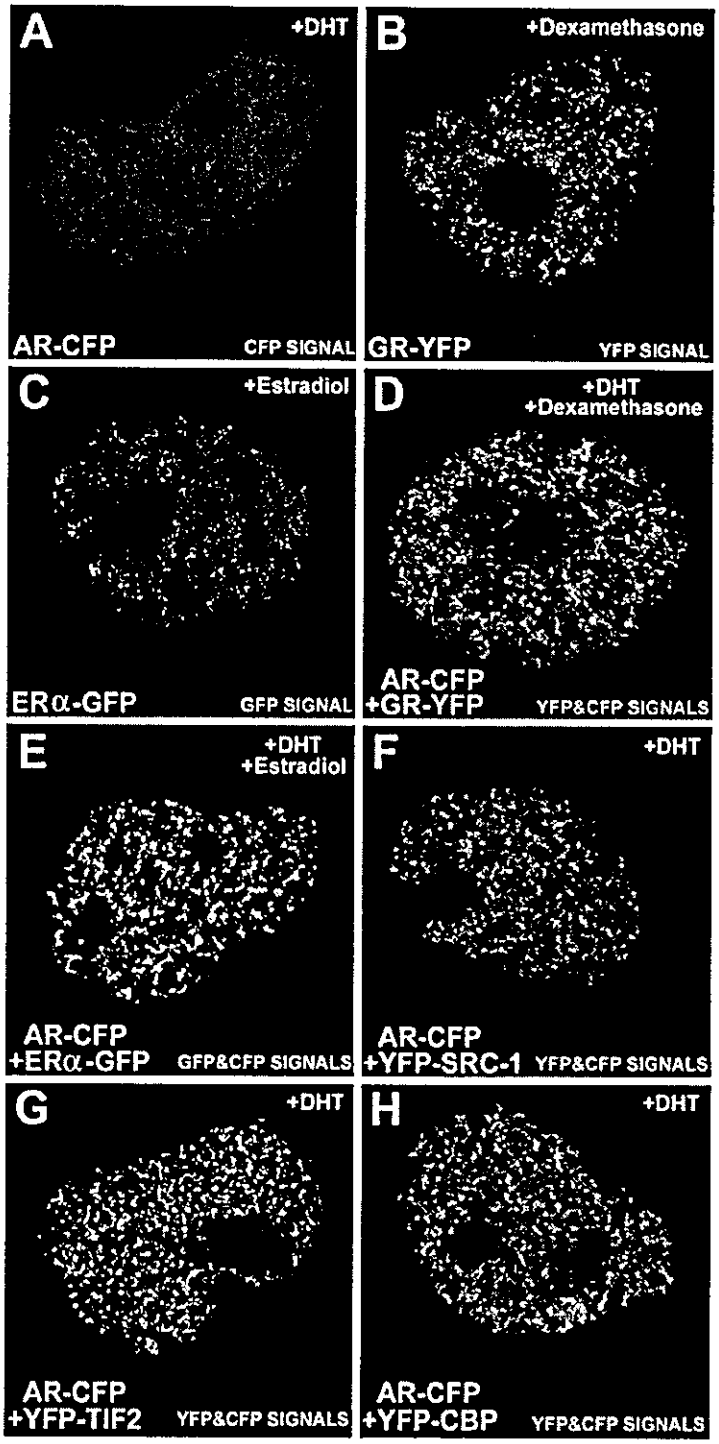

Fig. 7. The Three-Dimensional Image Analysis of the Intranuclear Localization of Liganded AR-CFP, GR-YFP and ERα-GFP, and YFP-Tagged Coactivators in COS7 Cells

COS7 cells were transfected with the expression plasmids indicated in each panel. In panel A, 0.25 μg of pCMV-AR-CFP was transfected, and the amounts of each plasmid transfected in other panels were equivalent on a molar basis. The cells were then scanned after treatment with 10^{-8} M ligand for each receptor as indicated. The images are displayed as surface views. The GFP, YFP, and CFP signals are represented as *green*, *yellow* and *red*, respectively. A, *Red* spots due to AR-CFP foci formation; B, *yellow* spots due to GR-YFP foci formation; C, *green* spots due to ERα-GFP foci formation; D, *orange*-colored foci formation by

thermore, YFP-SRC-1 (Fig. 7F), YFP-TIF2 (Fig. 7G) and YFP-CBP (Fig. 7H) were all colocalized with AR-CFP, forming identical spots.

DISCUSSION

The present study demonstrates that the coactivator CBP is involved in the intranuclear foci formation of AR. YFP-SRC-1 and YFP-TIF2 were homogenously distributed in the nucleus but converged to the foci of the DHT-bound AR-CFP upon cotransfection, whereas YFP-CBP was distributed in the nucleus in a fine speckled pattern but became colocalized with the liganded AR-CFP with an increased YFP intensity upon cotransfection (Fig. 2). The endogenous CBP was also distributed in a speckled pattern, and it was found, although indirectly, that the liganded AR-CFP bound to the endogenous CBP (Fig. 2, D–F). The introduction of a CBP mutant with a dominant negative effect on the AR-dependent transactivation destroyed the foci formation of AR-GFP, and AR-GFP was distributed in a uniform pattern. The involvement of CBP in the AR foci formation is also supported by reports that the addition of 12-*O*-tetradecanoylphorbol-13-acetate (20) or transfection of the expression plasmid for NF-κB (21) repressed the AR-dependent transactivation, and competition for endogenous CBP was speculated as the mechanism of this repression (20, 21). A diffuse intranuclear distribution of GFP-SRC-1 in cells transfected with the GFP-SRC-1 expression vector alone and a distribution of endogenous CBP in a microparticulate (finely speckled) pattern in nontransfected cells have also been reported by other groups (6, 22). A physiological significance of the difference in the intranuclear distribution between CBP and p160 coactivators such as SRC-1 and TIF2 remains unknown, but one of the speculations is as follows. CBP is an integrator of multiple signal transductions and interacts with various transcription regulators (12). Therefore, endogenous or exogenous CBP may make discrete foci by forming complexes with transcription factors other than the steroid receptors as well.

The AR is unusual among steroid hormone receptors in its AF-1 and AF-2 functions. Most of the transactivation functions of the AR exist in AF-1 in the NTD (16–19), and the ligand-dependent transactivation function of AF-2 in the LBD is extremely low in mammalian cells (15). In the absence of ligand, the LBD of the AR is thought to keep the AR retained in the cytosol (17) by masking the NLS, which was reported to exist within the DBD and the hinge region corresponding to amino acid residues 557–653 (23), 617–633 (17, 24), or 627–658 (25). The unliganded LBD has also been reported to suppress the constitutive transactivation function of the NTD (17, 23). The NTD of the AR has recently been shown to interact directly with TIF2 and SRC-1 (26, 27). The present study succeeded in perfectly visualizing these reports on AF-1 and AF-2 function in the AR (Fig. 4), as follows. Both the AR-AF-1-YFP and the AR-AF-2-CFP fragments prepared in the present study contained the exposed NLS, and therefore, each of them was translocated into the nucleus without ligand binding. The cotransfection of AR-AF-2-CFP and AR-AF-1-YFP suppressed the foci formation of AR-AF-1-YFP (Fig. 4C) and excluded the AR-AF-1-YFP to the cytosol (Fig. 4D). The transfection of AR-AF-1-YFP alone formed foci in the nucleus, reflecting its strong constitutive transactivation function, whereas the AR-AF-2-CFP alone did not produce foci even in the presence of ligand. YFP-SRC-1 and YFP-TIF2 were shown to be localized within the AR-AF-1-CFP foci (Fig. 4, K and L). The rapid recruitment of SRC-1 to the ERα foci upon exposure to E2 was studied by Stenoien *et al.* (6, 28), who reported that helix 12 and the AF-2 domain in the LBD are essential for the agonist-induced recruitment of coactivators, but the AF-1 domain and DBD are dispensable. In contrast to the ERα, AR-AF-1 can recruit SRC-1 and TIF2. Thus, the recruitment of coactivators is suggested to be an essential and common process for transactivation by the various steroid receptors, but the molecular mechanism is different among the receptors.

AR-AF-1 (NTD) and AR-AF-2 (LBD) showed a synergistic action. If the degree of transactivation of MMTV (mouse mammarian tumor virus) promoter induced by both AR-AF-1 (NTD) and liganded AR-AF-2 (LBD) is set at 100%, the transactivation induced by AR-AF-1 alone was 28% in COS7 cells, and that by liganded AR-AF-2 alone was less than 2% (Fig. 5). Similarly, the degree of transactivation by the AR NTD alone and by the liganded AR LBD alone have been reported to be 10–75% (18, 24, 29) and 0–3% (18, 19, 24, 25, 29), respectively, of that by the liganded wild-type AR in various types of cells. For an explanation of this synergistic mechanism, the following has been speculated. AR-AF-2, although its intrinsic activity is negligibly low, can associate with AR-AF-1 in the presence of ligand, and this intramolecular interaction results in the formation of a complete platform to recruit coactivators. This conformational change then elicits the full activity of the AR (19, 26, 27, 30–32). The above

AR-CFP and GR-YFP; E, *yellow*-colored foci formation by AR-CFP and ERα-GFP; F, G, and H, *orange*-colored foci formation by AR-CFP and YFP-tagged SRC-1, TIF2 or CBP, respectively. The numbers of spots identified as a distinct volume were quantified as 299 ± 63 (A), 301 ± 24 (B), 319 ± 22 (C), 303 ± 33 (D), 312 ± 30 (E), 262 ± 20 (F), 305 ± 27 (G), and 297 ± 23 (H) (mean ± SD) from four independent experiments.

speculation has been deduced from overall consideration of the results obtained by a reporter gene assay, a GST pull-down assay and a two-hybrid assay. If intramolecular interplay between the AF-1 and AF-2 domains really proceeds in living cells, there must be a difference between the structures of the receptor/coactivator complex in the case with AR-AF-1 alone *vs.* the case with full-length AR or the coexistence of AR-AF-1 and AR-AF-2. However, that difference was not detectable by two-dimensional image analysis. Therefore, a three-dimensional imaging method, which has recently been developed by us to detect accurately any antiandrogenic effect (9), was applied to the analyses of the subnuclear distribution of the fluorescent protein-tagged receptors. Using this method, to our knowledge, we for the first time succeeded in obtaining direct evidence of structural differences between the receptor/coactivator complex of AR-AF-1 alone and that of the full-length AR (Fig. 6, A and B). Three-dimensional imaging also revealed that the native AR/coactivator complexes, *i.e.* the AR foci, are distributed inside euchromatin, where transcription is thought to be active. This three-dimensional imaging method allowed analysis of the accurate subnuclear spatial localization and quantitation of the foci formed by the steroid hormone receptor labeled with fluorescent protein. The following was thus revealed. The AR, GR, and ERα were accumulated in identical subnuclear compartments in the presence of ligand. The maximum number of subnuclear compartments, which was considered to be observed with the overexpression of the steroid hormone receptors, *i.e.* with the transfection of their expression vectors, was approximately 300 in one COS7 cell nucleus. Coactivators such as SRC-1, TIF2, and CBP were also accumulated in the same subnuclear compartments with those of the steroid hormone receptors. An overexpression of these coactivators did not affect the maximum number of compartments. These findings might propose the hypothesis that transcriptionally activated steroid hormone receptors, regardless of the type of the receptor, are transferred to common compartments located in the euchromatin region and form a complex with coactivators. These receptor/coactivator complexes are then mobilized to the target genes of each receptor and are then rapidly returned to the compartment after use. This hypothesis would be supported by recent reports that liganded GFP-GR undergoes a rapid exchange between chromatin and the nucleoplasmic compartment (33) and that liganded GR and ERα are retained in the nuclear matrix even after DNase-digestion of the nucleus (6, 34). Furthermore, the dynamics of the ERα in the nucleus have recently been revealed by fluorescence recovery after photobleaching. It was shown that the E2-bound CFP-ERα/YFP-SRC-1 complex associates with the nuclear matrix (*i.e.* formation of foci) but undergoes rapid exchange within seconds (35).

In conclusion, the present study on the AR and foci formation in the nucleus provides novel findings regarding the physiological significance of the subnuclear foci formation of the steroid hormone receptors. CBP is at least one of the factors essential to foci formation of the AR. Foci formation indicates the formation of a complete steric conformation of the AR essential for transactivation, for which both the NTD and LBD are necessary, and is also evidence of the intranuclear compartmentalization that may be common to other steroid receptors and essential for full transcriptional activation. In addition, the three-dimensional imaging method performed in the present study seems to be an effective modality for further investigating the mechanism of nuclear receptor-mediated transcription.

MATERIALS AND METHODS

Plasmid Constructs

The firefly luciferase reporter vector (pGL3-MMTV) and the expression vectors for the human AR (pCMX-AR) (36), the C-terminal-truncated AR (AR-AF-1) corresponding to AR 1–703 (pCMX-AR-AF-1) and the N-terminal-truncated AR (AR-AF-2) corresponding to AR 502–919 (pCMX-AR-AF-2) were prepared as previously described (29). The expression plasmid for the DBD-deleted AR-AF-1 (Δ(DBD)AR-AF-1), corresponding to AR 1–501, was prepared by excising the DBD between *Hin*dIII and *Kpn*I sites of pCMX-AR-AF-1. The expression plasmids for the full-length mouse CBP 1–2443 (pcDNA/mCBP) and for the truncated mutants, pcDNA/mCBPΔ (118–2393), pcDNA/mCBPΔ (313–468), pcDNA/mCBPΔ (738–2393), and pcDNA/mCBPΔ (1570–1891), were prepared as previously described (37). Human cDNAs for the GR, SRC-1, and TIF2 were prepared as reported previously (29), and the human ERα cDNA was provided by Dr. Shigeaki Kato (Tokyo University, Japan). The expression plasmids for AR-GFP (pCMV-AR-GFP) and AR-CFP (pCMV-AR-CFP) chimeras were constructed by inserting the full-length AR cDNA into the *Nhe*I-*Sma*I sites of pEGFP-N1 and pECFP-N1 (CLONTECH Laboratories, Inc., Palo Alto, CA), respectively. The expression plasmids for AR-AF-1-YFP (pCMV-AR-AF-1-YFP) and AR-AF-2-CFP (pCMV-AR-AF-2-CFP) chimeras, in which fluorescent proteins were fused to the C termini of the AR fragments, were prepared by inserting the AR-AF-1 and AR-AF-2 cDNAs into the *Nhe*I-*Xho*I sites of pEYFP-N1 (CLONTECH Laboratories, Inc.) and the *Nhe*I-*Kpn*I sites of pECFP-N1, respectively, using PCR techniques. The expression plasmid for AR-AF-1-CFP (pCMV-AR-AF-1-CFP) was prepared by inserting the AR-AF-1 cDNA into the *Nhe*I-*Xho*I sites of pECFP-N1. Similarly, the expression plasmids for GR-YFP (pCMV-GR-YFP), ERα-GFP (pCMV-ERα-GFP), YFP-SRC-1 (pCMV-YFP-SRC-1), YFP-TIF2 (pCMV-YFP-TIF2) and Δ(DBD)AR-AF-1-YFP were constructed. The plasmids for YFP-AR-AF-1 (pCMV-YFP-AR-AF-1) and CFP-AR-AF-2 (pCMV-CFP-AR-AF-2), in which fluorescent proteins were fused to the N termini of the AR fragments, were prepared by inserting the AR-AF-1 and AR-AF-2 cDNAs into the *Nhe*I-*Xho*I sites of pEYFP-C1 and the *Bgl*II-*Xho*I sites of pECFP-C1 (CLONTECH Laboratories, Inc.), respectively. The expression vector for YFP-CBP chimera (pCMV-YFP-CBP) was constructed by inserting the YFP cDNA into the *Hin*dIII site of pcDNA/mCBP, upstream of the CBP sequence.

Reporter Assay

Kidney-derived cell lines, COS7 and CV-1, and a human prostatic cancer cell-line, LNCaP, were obtained from Amer-

ican Type Culture Collection (Manassas, VA). COS7 and CV-1 cells were maintained in DMEM (Life Technologies, Inc.) supplemented with 10% FBS, 2 mM L-glutamine and 100 U/ml of penicillin-streptomycin. LNCaP cells were similarly maintained except for the use of Roswell Park Memorial Institute 1640 medium instead of DMEM. The cells, cultured in 6-well plates (3×10^5 cells per well), were transfected with 1 μg/well of pGL3-MMTV as the reporter, 2 ng/well of pRL-CMV (a Renilla luciferase vector, Promega Corp., Madison, WI) as the internal control, and 0.1 to 0.2 μg/well of the expression vector for the AR, the AR fragment, the chimeric receptor or the mutated CBP, using 7 μl/well of SuperFect reagent (QIAGEN, Hilden, Germany). For coexpression studies, the total amount of vector added to each well was equalized by the addition of empty vector, unless otherwise indicated. Starting 3 h after transfection, the cells were incubated for 48 h in DMEM with 10% charcoal-treated FBS in the presence or absence of 10^{-8} M 5α-dihydrotestosterone, 10^{-8} M dexamethasone, 10^{-8} M E2, or 10^{-6} M OHF. The cells were then solubilized with 500 μl of lysis buffer (Promega Corp.) and the activities of the reporter gene were determined by the Dual-Luciferase Reporter Assay System (Promega Corp.). One-way analysis of variance followed by Scheffé's test was used for multi-group comparisons.

Fluorescence Microscopy and Three-Dimensional Image Analysis

The cells were cultured in 35-mm glass-bottom dishes (MatTek) (3×10^5 cells/dish) and then transfected with various plasmids in a total amount of 0.5 μg/dish using 2.5 μl of SuperFect. For coexpression studies, the total amount of vector added to each dish was equalized by the addition of empty vector, unless otherwise indicated. Sixteen to 24 h after incubation in DMEM containing 10% charcoal-treated FBS, the culture media were replaced with fresh DMEM in the presence or absence of the hormones or chemicals, and then the cells were observed with a Leica Corp. TSP-SP invert confocal laser scanning microscope (Leica Corp. Microsystems, Heidelberg, Germany), using a 100×, 1.4 numerical aperture PL APO oil immersion objective. Imaging for GFP, YFP, and CFP was performed by excitation with the 488-nm, 514-nm, and 450-nm lines, respectively, from an argon laser, and the emissions were viewed through band passes ranging from 500 to 550 nm, from 530 to 590 nm, and from 470 to 500 nm, respectively, by band pass regulation with a Prism System (Leica Corp. Microsystems). For simultaneous imaging of multiple fluorescent proteins, the laser line was changed, and the band pass was further finely controlled so as not to overlap emissions. For example, for the simultaneous observation of AR-CFP and ERα-GFP, the chimeras were imaged by excitation with 450-nm and 514-nm lines, respectively, and the emissions through band passes ranging from 460 to 480 nm and from 580 to 620 nm, respectively, were observed. The nuclei were stained with Hoechst 33342 (Molecular Probes, Inc., Eugene, OR) (2 μg/ml) and excited with the 350-nm line from a UV laser, and the emission was viewed through a band pass ranging from 400 to 450 nm. For immunostaining, the cells were washed using PBS and fixed in 4% (vol/vol) paraformaldehyde in PBS for 30 min at 25 C. After being blocked in 10% goat serum for 1 h, the cells were incubated with anti-CBP mouse monoclonal antibody [CBP (C-1) against the C terminus of CBP] or anti-CBP rabbit polyclonal antibodies [CBP (A-22) against the N terminus and CBP (451) against the CREB-binding domain] (Santa Cruz Biotechnology, Inc., Santa Cruz, CA) at 1:100-fold dilution for 1 h, followed by incubation with 0.33 μg/ml of Alexa Fluor 594-labeled antimouse or antirabbit IgG or Alexa Fluor 488-labeled antirabbit IgG (Molecular Probes, Inc.) for 1 h at 25 C. After being washed by PBS, the stained cells were observed with a confocal microscope by excitation with the 568-nm line from a krypton laser and emission from 600–640 nm for Alexa Fluor 594-labeled IgG or by excitation with the 514-nm line from an argon laser and emission from 520 to 560 nm for Alexa Fluor 488-labeled IgG. A three-dimensional imaging study was performed essentially in the same manner as previously reported (9). In brief, a series of 30–50 scanning images were collected for each single nucleus, and these two-dimensional tomograms were reconstructed using the three-dimensional analysis software of TRI Graphics Program (Ratoc System Engineering, Tokyo, Japan). Both the spatial distribution and calculations of the fluorescent proteins as a distinct volume were made possible by removing scattering background fluorescence and lens spherical aberrations and then by separating each particle.

Acknowledgments

This work was performed in part at the Kyushu University Station for Collaborative Research. The authors gratefully thank Mitoshi Toki for his valuable technical assistance in performing the three-dimensional imaging analyses, and Pamela J. Tamura for assistance in preparing the manuscript.

Received July 17, 2001. Accepted December 14, 2001.

Address all correspondence and requests for reprints to: Hajime Nawata, M.D., Ph.D., Department of Medicine and Bioregulatory Science, Graduate School of Medical Sciences, Kyushu University, Maidashi 3-1-1, Higashi-ku, Fukuoka 812-8582, Japan. E-mail: nawata@intmed3.med.kyushu-u.ac.jp.

This work was supported in part by a Grant-in-Aid for Scientific Research from The Ministry of Education, Science, Sports and Culture, Japan.

REFERENCES

1. Ogawa H, Inouye S, Tsuji FI, Yasuda K, Umesono K 1995 Localization, trafficking, and temperature-dependence of the Aequorea green fluorescent protein in cultured vertebrate cells. Proc Natl Acad Sci USA 92:11899–11903
2. Htun H, Barsony J, Renyi I, Gould DL, Hager GL 1996 Visualization of glucocorticoid receptor translocation and intranuclear organization in living cells with a green fluorescent protein chimera. Proc Natl Acad Sci USA 93: 4845–4850
3. Georget V, Lobaccaro JM, Terouanne B, Mangeat P, Nicolas J-C, Sultan C 1997 Trafficking of the androgen receptor in living cells with fused green fluorescent protein-androgen receptor. Mol Cell Endocrinol 129: 17–26
4. Fejes-Tóth G, Pearce D, Náray-Fejes-Tóth A 1998 Subcellular localization of mineralocorticoid receptors in living cells: effects of receptor agonists and antagonists. Proc Natl Acad Sci USA 95:2973–2978
5. Htun H, Holth LT, Walker D, Davie JR, Hager GL 1999 Direct visualization of the human estrogen receptor reveals a role for ligand in the nuclear distribution of the receptor. Mol Biol Cell 10:471–486
6. Stenoien DL, Mancini MG, Patel K, Allegretto EA, Smith CL, Mancini MA 2000 Subnuclear trafficking of estrogen receptor-α and steroid receptor coactivator-1. Mol Endocrinol 14:518–534
7. Racz A, Barsony J 1999 Hormone-dependent translocation of vitamin D receptors is linked to transactivation. J Biol Chem 274:19352–19360
8. Tyagi RK, Lavrovsky Y, Ahn SC, Song CS, Chatterjee B, Roy AK 2000 Dynamics of intracellular movement and nucleocytoplasmic recycling of the ligand-activated androgen receptor in living cells. Mol Endocrinol 14: 1162–1174

9. Tomura A, Goto K, Morinaga H, Nomura M, Okabe T, Yanase T, Takayanagi R, Nawata H 2001 The subnuclear three dimensional image analysis of androgen receptor fused to green fluorescence protein. J Biol Chem 276: 28395–28401
10. Beato M, Herrlich P, Schutz G 1995 Steroid hormone receptors: many actors in search of a plot. Cell 83: 851–857
11. Horwitz KB, Jackson TA, Bain DL, Richer JK, Takimoto GS, Tung L 1996 Nuclear receptor coactivators and corepressors. Mol Endocrinol 10:1167–1177
12. Kamei K, Xu L, Heinzel T, Torchia J, Kurokawa R, Gloss B, Lin S-C, Heyman RA, Rose DW, Glass CK, Rosenfeld MG 1996 A CBP integrator complex mediates transcriptional activation and AP-1 inhibition by nuclear receptors. Cell 85: 403–414
13. Onate SA, Tsai SY, Tsai M-J, O'Malley BW 1995 Sequence and characterization of a coactivator for the steroid hormone receptor superfamily. Science 270: 1354–1357
14. Voegel JJ, Heine MJS, Zechel C, Chambon P, Gronemeyer H 1996 TIF2, a 160 kDa transcriptional mediator for the ligand-dependent activation function AF-2 of nuclear receptors. EMBO J 15:3667–3675
15. Moilanen A, Rouleau N, Ikonen T, Palvimo JJ, Jänne OA 1997 The presence of a transcription activation function in the hormone-binding domain of androgen receptor is revealed by studies in yeast cells. FEBS Lett 412: 355–358
16. Rundlett SE, Wu XP, Miesfeld RL 1990 Functional characterizations of the androgen receptor confirm that the molecular basis of androgen action is transcriptional regulation. Mol Endocrinol 4:708–714
17. Zhou ZX, Sar M, Simental JA, Lane MV, Wilson EM 1994 A ligand-dependent bipartite nuclear targeting signal in the human androgen receptor. Requirement for the DNA-binding domain and modulation by NH2-terminal and carboxyl-terminal sequences. J Biol Chem 269: 13115–13123
18. Jenster G, van der Korput H AGM, Trapman J 1995 Identification of two transcription activation units in the N-terminal domain of the human androgen receptor. J Biol Chem 270:7341–7346
19. Ikonen T, Palvimo JJ, Jänne OA 1997 Interaction between the amino- and carboxyl-terminal regions of the rat androgen receptor modulates transcriptional activity and is influenced by nuclear receptor coactivators. J Biol Chem 272:29821–29828
20. Frønsdal K, Engedal N, Slagsvold T, Saatcioglu F 1998 CREB binding protein is a coactivator for the androgen receptor and mediates cross-talk with AP-1. J Biol Chem 273:31853–31859
21. Aarnisalo P, Palvimo JJ, Jänne OA 1998 CREB-binding protein in androgen receptor-mediated signaling. Proc Natl Acad Sci USA 95:2122–2127
22. LaMorte VJ, Dyck JA, Ochs RL, and Evans RM 1998 Localization of nascent RNA and CREB binding protein with the PML-containing nuclear body. Proc Natl Acad Sci USA 95:4991–4996
23. Jenster G, van der Korput HA, van Vroonhoven C, van der Kwast TH, Trapman J, Brinkmann AO 1991 Domains of the human androgen receptor involved in steroid binding, transcriptional activation, and subcellular localization. Mol Endocrinol 5:1396–1404
24. Poukka H, Karvonen U, Yoshikawa N, Tanaka H, Palvimo JJ, Jänne OA 2000 The RING finger protein SNURF modulates nuclear trafficking of the androgen receptor. J Cell Sci 113:2991–3001
25. Simental JA, Sar M, Lane MV, French FS, Wilson EM 1991 Transcriptional activation and nuclear targeting signals of the human androgen receptor. J Biol Chem 266: 510–518
26. Alen P, Claessens F, Verhoeven G, Rombauts W, Peeters B 1999 The androgen receptor amino-terminal domain plays a key role in p160 coactivator-stimulated gene transcription. Mol Cell Biol 19:6085–6097
27. Bevan CL, Hoare S, Claessens F, Heery DM, Parker MG 1999 The AF1 and AF2 domains of the androgen receptor interact with distinct regions of SRC1. Mol Cell Biol 19:8383–8392
28. Stenoien DL, Nye AC, Mancini MG, Patel K, Dutertre M, O'Malley BW, Smith CL, Belmont AS, and Mancini MA 2001 Ligand-mediated assembly and real-time cellular dynamics of estrogen receptor-coactivator complexes in living cells. Mol Cell Biol 21:4404–4412
29. Adachi M, Takayanagi R, Tomura A, Imasaki K, Kato S, Goto K, Yanase T, Ikuyama S, Nawata H 2000 Androgen-insensitivity syndrome as a possible coactivator disease. N Engl J Med 343:856–862
30. Doesburg P, Kuil CW, Berrevoets CA, Steketee K, Faber PW, Mulder E, Brinkmann AO, Trapman J 1996 Functional *in vivo* interaction between the amino-terminal, transactivation domain and the ligand binding domain of the androgen receptor. Biochemistry 36:1052–1064
31. Berrevoets CA, Doesburg P, Steketee K, Trapman J, Brinkmann AO 2012 1998 Functional interactions of the AF-2 activation domain core region of the human androgen receptor with the amino-terminal domain and with the transcriptional coactivator TIF2 (transcriptional intermediary factor 2). Mol Endocrinol 12:1172–1183
32. He B, Kemppainen JA, Wilson EM 2000 FXXLF and WXXLF sequences mediate the NH2-terminal interaction with the ligand binding domain of the androgen receptor. J Biol Chem 275:22986–22994
33. McNally JG, Müller WG, Walker D, Wolford R, Hager GL 2000 The glucocorticoid receptor: rapid exchange with regulatory sites in living cells. Science 287:1262–1265
34. van Steensel B, Brink M, van der Meulen K, van Binnendijk EP, Wansink DG, de Jong L, de Kloet ER, van Driel R 1995 Localization of the glucocorticoid receptor in discrete clusters in the cell nucleus. J Cell Sci 108: 3003–3011
35. Stenoien DL, Patel K, Mancini MG, Dutertre M, Smith CL, O'Malley BW, Mancini MA 2001 FRAP reveals that mobility of oestrogen receptor-α is ligand- and proteasome-dependent. Nat Cell Biol 3:15–23
36. Nakao R, Haji M, Yanase T, Ogo A, Takayanagi R, Katsube T, Fukumaki Y, Nawata H 1992 A single amino acid substitution (Met^{786}→Val) in the steroid-binding domain of human androgen receptor leads to complete androgen insensitivity syndrome. J Clin Endocrinol Metab 74: 1152–1157
37. Miyagishi M, Fujii R, Hatta M, Yoshida E, Araya N, Nagafuchi A, Ishihara S, Nakajima T, Fukamizu A 2000 Regulation of Lef-mediated transcription and p53-dependent pathway by associating β-catenin with CBP/p300. J Biol Chem 275:35170–35175

THE JOURNAL OF BIOLOGICAL CHEMISTRY
Vol. 277, No. 33, Issue of August 16, pp. 30031–30039, 2002
Printed in U.S.A.

Activation Function-1 Domain of Androgen Receptor Contributes to the Interaction between Subnuclear Splicing Factor Compartment and Nuclear Receptor Compartment

IDENTIFICATION OF THE p102 U5 SMALL NUCLEAR RIBONUCLEOPROTEIN PARTICLE-BINDING PROTEIN AS A COACTIVATOR FOR THE RECEPTOR*

Received for publication, April 19, 2002, and in revised form, May 29, 2002
Published, JBC Papers in Press, May 30, 2002, DOI 10.1074/jbc.M203811200

Yue Zhao‡, Kiminobu Goto‡§, Masayuki Saitoh‡, Toshihiko Yanase‡§, Masatoshi Nomura‡, Taijiro Okabe‡, Ryoichi Takayanagi§, and Hajime Nawata‡§¶

From the ‡Department of Medicine and Bioregulatory Science (3rd Department of Internal Medicine), Graduate School of Medical Sciences, Kyushu University, Maidashi 3-1-1, Higashi-ku, Fukuoka 812-8582, and §Core Research for Evolutional Science and Technology (CREST), Japan Science and Technology Corporation, Hon-machi 4-1-8, Kawaguchi, Saitama 332-0012, Japan

In the androgen receptor (AR), most of its transactivation activity is mediated via the activation function-1 (AF-1). By employing yeast two-hybrid assay, we isolated a cDNA sequence encoding a protein binding to AR-AF-1. This protein, named ANT-1 (AR N-terminal domain transactivating protein-1), enhanced the ligand-independent autonomous AF-1 transactivation function of AR or glucocorticoid receptor but did not enhance that of estrogen receptor α. In contrast, the ANT-1 did not enhance any ligand-dependent AF-2 activities. Furthermore, the ligand-independent interaction between AR-AF-1 and ANT-1 was confirmed *in vivo* and *in vitro*. The ANT-1 sequence was identical to that of a protein that binds to U5 small nuclear ribonucleoprotein particle, a human homologue of yeast splicing factor Prp6p, involved in spliceosome. ANT-1 was compartmentalized into 20–40 coarse splicing factor compartment speckles against the background of the diffuse reticular distribution. AR colocalized with ANT-1 only in the diffusely distributed area, whereas the ANT-1 speckles were spatially distinct from but surrounded by the AR compartments. The active gene transcription has been shown to couple simultaneously with pre-mRNA processing at the periphery of the splicing factor compartment. The molecular interaction between two spatially distinct subnuclear compartments mediated by ANT-1 may therefore recruit AR into the transcription-splicing-coupling machinery.

Steroid hormone receptors contain the following three functional domains: a variable N-terminal transactivating domain, a highly conserved DNA binding domain, and a moderately well conserved C-terminal ligand binding domain (1, 2). AR,[1] like other members of the superfamily, harbors the following two transcription activation functions (AF): constitutively active AF-1 located in the N-terminal transactivating domain of the receptor, and a ligand-dependent AF-2 within the ligand binding domain (3). A number of transcriptional cofactors (coactivator or corepressor) have been identified that associate, in a ligand-dependent fashion, with the AF-2 regions of the steroid hormone receptors. They include the p160 family (4–7), CBP/p300 (8), PCAF/GCN5 (9), and TRAPs/DRIPs (10). These transcriptional cofactors are organized in multiprotein complexes and facilitate the access of nuclear receptors and the RNA polymerase II core machinery to their target DNA sequences by chromatin remodeling and histone modification. In addition to these transcription cofactors interacting with many nuclear receptors, HBO1 (11), ARA54, ARA55, ARA70, (12–16), p21-activated kinase PAK6 (17), Caveolin 1 (18), Tip60 (19), and FHL2 (20) have been identified as ligand-dependent AR-associated cofactors.

AR has been thought to be quite unique among the nuclear receptor superfamily members, because most, if not all, of its activities are mediated via the ligand-independent constitutive activity of AF-1 function (21, 22). This is in strong contrast to estrogen receptor α (ERα), in which the overall transactivation capacities are primarily dependent on AF-2 (23). In addition, the interaction of the N- and C-terminal domain is important for exerting the full AR transactivation capacity (21, 24, 25). The AR shares the hormone-response element sequences on the DNA with the receptors for glucocorticoid (GR), mineralocorticoid, and progesterone (26). In this regard, the N-terminal region, which varies among these receptors, is also thought to be responsible for the cell- and ligand- specific regulation of their target genes (27). In addition to p300/CBP (8) and SRC-1 (21), which interact with both AF-1 and AF-2, ARA24 (12), ARA160 (16), cdk-activating kinase (28), ART-27 (29), breast cancer susceptibility gene 1 (*BRCA1*) (30), SRA (31), and cyclin E (32) have also been proposed to bind to AR N-terminal transactivating domain. Among these cofactors, cyclin E is known to interact with U2 Small nuclear ribonucleoprotein particle

* This work was in part supported by a grant-in-aid for Scientific Research from The Ministry of Education, Culture, Sports, Science, and Technology, Japan. The costs of publication of this article were defrayed in part by the payment of page charges. This article must therefore be hereby marked "*advertisement*" in accordance with 18 U.S.C. Section 1734 solely to indicate this fact.

¶ To whom correspondence should be addressed: Dept. of Medicine and Bioregulatory Science (3rd Department of Internal Medicine), Graduate School of Medical Sciences, Kyushu University, Maidashi 3-1-1, Higashi-ku, Fukuoka 812-8582, Japan. Tel.: 81-92-642-5280; Fax: 81-92-642-5297; E-mail: nawata@intmed3.med.kyushu-u.ac.jp.

[1] The abbreviations used are: AR, androgen receptor; AF-1, activation function-1; ANT-1, androgen receptor N-terminal domain transactivating protein-1; snRNP, small nuclear ribonucleoprotein particle; ERα, estrogen receptor α; GR, glucocorticoid receptor; MMTV, mouse mammary tumor virus; DHT, dihydrotestosterone; GST, glutathione *S*-transferase; YFP, yellow fluorescence protein; CFP, cyan fluorescence protein; TPR, tetratricopeptide repeats; CBP, CREB-binding protein; CREB, cAMP-response element-binding protein; aa, amino acids; DTT, dithiothreitol; snRNP, small nuclear ribonucleoprotein.

(snRNP) (33), thus suggesting that AR-AF-1 might be involved in the pre-mRNA splicing mechanisms. The fundamental role of AR-AF-1 was also further supported by our recent clinical finding (34) showing that the absence of an AR-AF-1-specific transcription coactivator resulted in androgen insensitivity syndrome.

We isolated a cDNA sequence that encoded a protein named ANT-1 (androgen receptor N-terminal domain transactivating protein-1) as the AR-AF-1-binding protein. The ANT-1 was identical to a protein that binds to a human splicing factor U5 snRNP, a human homologue of yeast splicing factor prp6p (35, 36) compartmentalized with the yeast spliceosomal penta-snRNP (37). By using a three-dimensional reconstruction of the confocal microscopic images, the spatial interrelationship between two distinct subnuclear compartments, one formed by steroid hormone receptors and another by splicing factors, was elucidated.

EXPERIMENTAL PROCEDURES

Plasmids—pEYFP-ANT1 and pANT-myc were constructed by inserting the ANT-1 cDNA into *Kpn*I and *Sma*I sites of pEYFP-C2 (CLONTECH) and *Kpn*I and *Not*I sites of pcDNA3-myc-his, respectively. pCMVhAR, pCMXhAR-(1–703 aa), pCMXhAR-(502–919 aa), pCMXhGR, pCMXhGR-(1–550 aa), pCMXhGR-(415–777 aa), pGEX-AR, pGEX-AR-(1–532 aa), pGEX-GR-(13–438 aa), and the reporter plasmid pMMTV-luc, containing the luciferase gene driven by mouse mammary tumor virus (MMTV) long terminal repeat harboring hormone-response element for both AR and GR, have been described previously (34). The human aromatase gene fragment encompassing exon Ib and the upstream promoter region (38) (−1101 to +60, containing the glucocorticoid response element at −333 to −319) was subcloned into pGL3-luc (CLONTECH), thus creating pAROM-luc. The expression plasmids for human ERα (pSG5-ERα) and a reporter plasmid for ERα (pERE2-tk109-luc), pGEX-4T-ERα-(29–180 aa), and pGEX-4T-ERα-(282–595 aa) were provided by Dr. Shigeaki Kato (University of Tokyo, Japan). The expression plasmid for human cyclin E was provided by Dr. Makoto Nakanishi (Nagoya City University, Japan).

Isolation of ANT-1 by Swapped Yeast Two-hybrid Screening and Northern Blot—MatchMaker Plus (CLONTECH) was used for the yeast two-hybrid screening. Poly(A) RNA was isolated from primary cultured human skin fibroblasts. cDNA library was constructed using TimeSaver cDNA Synthesis Kit (Amersham Biosciences) with random primers (Amersham Biosciences) and was inserted into pLexA-BD included in the MatchMaker Plus kit. A cDNA fragment, used for bait, encoding N-terminal transactivating domain (1–532-aa residue) of human AR was ligated in-frame into pB42-AD, thus creating pB42-AD-AF1-expressing AR-AF-1 fused to the GAL1 activation domain. The yeast EGY48 strain was transformed with the pLexA-BD carrying the human fibroblast cDNA libraries and with the pB42-AD-AF1 according to the manufacturer's protocol, and thereafter the transformants were selected on an appropriate nutrition medium. Positive candidate plasmids for AR-AF-1-binding proteins were recovered from the yeast, and the nucleotide sequences were determined using the ABI PRISM 377 DNA Sequencer (PerkinElmer Life Sciences). The specificity of interaction was further confirmed by a liquid galactosidase assay. To obtain full-length ANT-1 cDNA, the partial cDNA fragment encoding 78–495-aa residues of ANT-1, obtained by the two-hybrid screening, was ^{32}P-labeled as a probe for the screening of human prostate cDNA library carried by a λgt10 phage vector (CLONTECH). The full-length ANT-1 cDNA was ligated into pcDNA3 to create pcDNA3-ANT-1. For the Northern blot analysis, MTN blots were purchased from CLONTECH. A DNA fragment covering 463–703 amino acids of ANT-1 was labeled as a probe with [α-^{32}P]dCTP by the random priming method. Prehybridization and hybridization were performed according to the manufacturer's protocol.

Cell Culture, Transient Transfection Assay—COS-7 and ALVA-41 prostatic cancer cells (5×10^5 cells per well in 6-well plate), cultured in Dulbecco's modified Eagle's medium supplemented with 10% fetal calf serum, were transiently transfected using a Superfect Transfection Kit (Invitrogen). Generally, 2.5 μg of plasmid DNA (0.2–1.0 μg of pcDNA3-ANT-1, 0.2 μg of pCMVhAR, 1.0 μg of pMMTV-luc) per well were used for the transfection, whereas the total amounts of the transfected DNA were kept constant by adding pcDNA3 plasmid. At 16 h post-transfection, the cells were rinsed and re-fed with medium containing 10% charcoal-stripped fetal calf serum with or without steroid hormones (10^{-8} M dihydrotestosterone (DHT) or 17β-estradiol, and 10^{-7} M dexamethasone, respectively). After an additional 18 h, the cells were harvested and assayed for luciferase activities using the Dual-Luciferase Reporter Assay System (Promega).

Protein-Protein Interaction Using GST Chimeric Proteins—Full-length AR (AR-(1–919)) fused to glutathione *S*-transferase (GST) was expressed in Sf9 insect cells, thus generating GST-AR-(1–919). GST fusions with AR-(1–532), AR-(564–919), AR-(622–919), GR-(13–438), GR-(421–777), GR-(486–777), ERα-(29–180), and ERα-(282–595) were expressed in *Escherichia coli*. *In vitro* transcription and translation were performed using the TNT-coupled Reticulocyte Lysate System (Promega) and pcDNA3-ANT as a template. For the GST pull-down analysis, GST fusion proteins coupled to glutathione-Sepharose beads (Amersham Biosciences) were incubated with ^{35}S-labeled ANT-1 at 4 °C for 2 h in the NETN buffer (0.2% Nonidet P-40, 1 mM EDTA, 20 mM Tris-Cl, pH 7.8, 200 mM NaCl, 5% glycerol, 1 mM DTT, 1 tablet of protease inhibitor mixture (Roche Molecular Biochemicals)). The pellets were washed 5 times in a washing buffer (replacing 200 mM NaCl in NETN buffer with 500 mM NaCl) and resuspended in an SDS-PAGE sample buffer. The radiolabeled proteins were detected with STORM860 image analyzer (Amersham Biosciences).

Immunoprecipitations—For the immunocoprecipitation analysis, COS-7 cells were transfected with plasmids expressing Myc-tagged ANT-1 and full-length or truncated AR and were maintained with or without 10^{-8} M DHT. Whole cell lysates were prepared by lysing cells in a buffer (1.0% Nonidet P-40, 50 mM Tris-Cl, pH 7.8, 150 mM NaCl, 1 mM DTT, 1 tablet of protease inhibitor mixture). In one experiment, nuclear lysates were prepared as described previously (39). The lysates were incubated at 4 °C for 1 h with the antibody against c-*myc* (Santa Cruz Biotechnology) in immunoprecipitation (IP) buffer (0.5% Nonidet P-40, 1 mM EDTA, 50 mM Tris-Cl, pH 7.8, 200 mM NaCl, 1 mM DTT, 1 tablet of protease inhibitor mixture) and then were further incubated with protein-A-Sepharose beads (Amersham Biosciences) at 4 °C for 2 h. A Western blot analysis was performed using either antibody N-20 (Santa Cruz Biotechnology) to detect the full-length or N-terminal transactivating domain fragment of AR or using antibody C-19 (Santa Cruz Biotechnology) to detect the C-terminal fragment.

Microscopy and Imaging Analysis—The COS-7 cells were divided into 35-mm glass-bottom dishes (MatTek Corp.) and then were transfected with 0.5 μg of pAR-CFP and pANT-1-YFP using 2.5 μl/dish of Superfect reagents (Qiagen). Six to 18 h post-transfection, the culture medium was replaced with a fresh Dulbecco's modified Eagle's medium containing 10^{-8} M DHT. One hour after adding DHT, the cells were scanned using a Leica TCS-SP system (Leica Microsystems, Heidelberg, Germany) as described previously (40). The cells were imaged for yellow or cyan fluorescence by excitation with the 514 and 450 nm line, respectively, from an argon laser. The emissions were viewed through either a 530–590-nm bandpass filter for yellow fluorescence protein (YFP) or a 470–500-nm bandpass filter for cyan fluorescence protein (CFP). The nuclei were stained with Hoechst 33342 (2 μg/ml) and were imaged by excitation with the 350-nm line from an ultraviolet laser, and the emission was viewed through a 400–450-nm bandpass filter. A series of 30–50 images were collected for each single nucleus. In each plane, the cyan, yellow, and ultraviolet fluorescence were consecutively collected using serial scanning methods equipped in Leica TCS-SP system. Three-dimensional image reconstruction was performed using either the three-dimensional analysis TRI Graphics Program software package (Ratoc System Engineering, Tokyo) (40) or the deconvolution method (nearest neighbors).

RESULTS

Isolation of ANT-1 with Swapped Yeast Two-hybrid Screening—To identify the cDNA encoding proteins binding to AR-AF-1 sequence, we performed a yeast two-hybrid screening. Because AR-AF-1 possesses a strong autonomous transactivation capacity, we could not use pLexA-BD, which is regularly used as the bait protein plasmid vector. Instead, we inserted AR-AF-1 cDNA into pB42-AD, and cDNA libraries representing human skin fibroblast mRNAs were carried by the pLexA-BD. By employing this "swapped" modification, the background false-positive blue colonies representing the transactivation capacities of the bait protein in yeast strain EGY48 became very weak, thus allowing us to perform the two-hybrid screening. Although during the second and the third screens retesting the specific ability of the candidate clones was critical, about

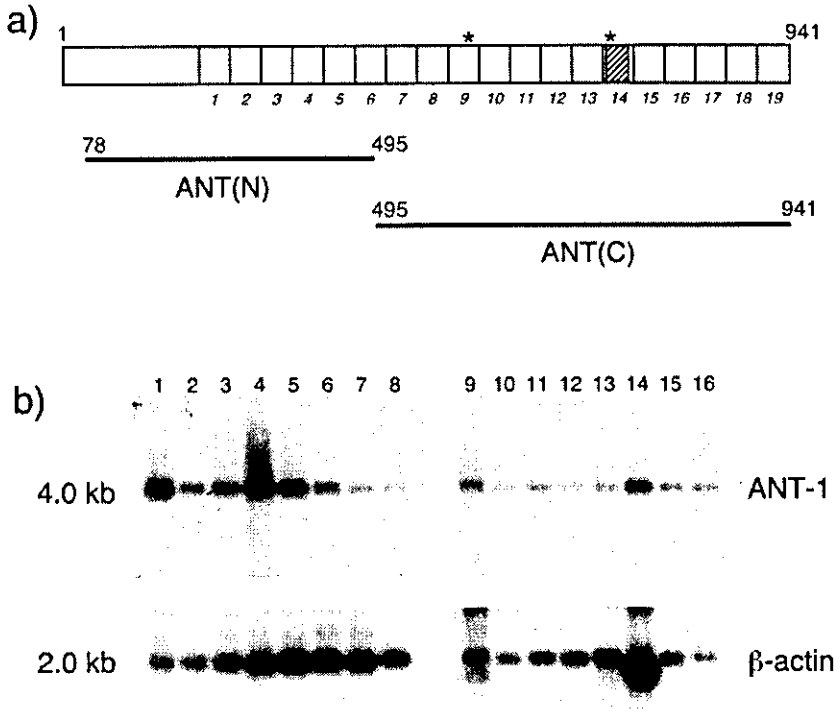

FIG. 1. *a*, schematic representation of the structure of ANT-1. ANT-1 contains 19 TPR elements in a tandem fashion, two LXXLL motifs, and one leucine zipper motif (TPRs, *small open boxes* numbered *1–19*; LXXLL motifs, *asterisks*; leucine zipper motif, *dashed box*, respectively). Note that the leucine zipper motif is within the 14th TPR motif. The structures of the plasmids expressing the truncated mutants are also shown. *b*, tissue distribution of ANT-1. The 4.0-kb mRNAs of ANT-1 are ubiquitously expressed among all the tissues examined. Lanes are as follows: *lane 1*, spleen; *lane 2*, thymus; *lane 3*, prostate; *lane 4*, testis; *lane 5*, ovary; *lane 6*, small intestine; *lane 7*, colon; *lane 8*, peripheral blood leukocyte; *lane 9*, heart; *lane 10*, brain; *lane 11*, placenta; *lane 12*, lung; *lane 13*, liver; *lane 14*, skeletal muscle; *lane 15*, kidney; and *lane 16*, pancreas, respectively. The *lower panels* show the same blots reprobed with human β-actin cDNA.

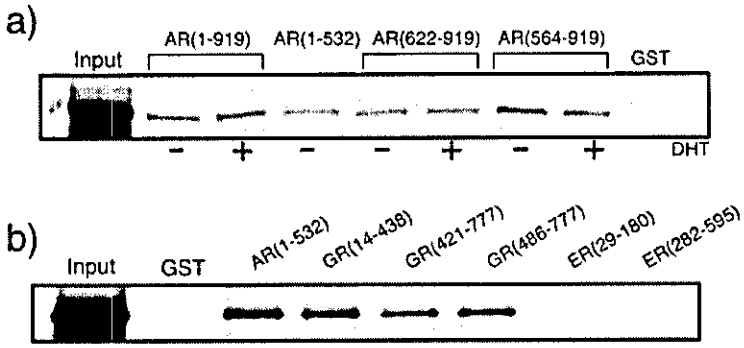

FIG. 2. *a*, *in vitro* binding of ANT-1 with AR. AR fragments fused to GST were subjected to GST pull-down analysis with or without the presence of 10^{-8} M DHT. *AR-(1–919)*, full-length AR; *AR-(1–532)*, AR-AF-1; *AR-(622–919)*, AR-AF-2; *AR-(564–919)*, DNA binding domain plus AR-AF-2. *b*, *in vitro* binding of ANT-1 with truncated mutants of GR or ER. Truncated mutants of GR or ER fused to GST were subjected to a GST pull-down analysis. The reactions were performed without ligands.

2×10^5 independent clones were subjected to the screening. We identified one positive clone harboring ~1.3 kb of the open reading frame, and then this fragment was used to obtain the full-length cDNA. The translation of the coding sequence revealed that the putative protein consisted of 941-aa residues with a predicted molecular mass of 102 kDa, which was named ANT-1. The homology search of the known amino acid sequences revealed that ANT-1 was identical to a nucleoprotein that binds to a human splicing factor U5 snRNP (GenBank™ accession number AF221842) (35, 36). ANT-1 contains 19 tetratricopeptide repeats (TPR) elements, two LXXLL motifs (41), and one leucine zipper motif (Fig. 1*a*) (42). Typically, the TPR motif appears in a tandem array and thus provides the scaffolds to mediate protein-protein interactions (43). A Northern blot analysis revealed the ANT-1 sequence to be ubiquitously expressed among the tissues examined (Fig. 1*b*).

Protein-Protein Interactions between ANT-1 and AR, GR, and ER—To confirm the binding capacities of ANT-1 with AR-AF-1, a GST pull-down analysis was performed using a series of GST-fused fragments of AR (Fig. 2*a*), GR, or ERα (Fig. 2*b*). Ligand-independent binding was observed, not only for full-length AR-(1–919) but also for AR-(1–532) covering AF-1, AR-(622–919) covering the ligand binding domain, or AR-(564–919) covering DNA binding domain and ligand binding domain. Furthermore, ANT-1 interacted with GR. The truncated GR fragments, such as GR-(14–438) covering AF-1, GR-(486–777) covering ligand binding domain, and GR-(421–777) covering ligand binding domain and DNA binding domain, were bound to ANT-1 without ligand. No significant difference was observed between the incubations with or without specific ligands. In contrast, two fragments covering ER-(29–180) for the AF-1 of ERα or ER-(282–595) for the AF-2 region failed to bind to ANT-1. The addition of 17β-estradiol did not promote such binding (data not shown).

Next, immunocoprecipitation experiments using either whole cell extracts (Fig. 3, *a*, *c*, and *d*) or nuclear extracts (Fig. 3*b*) were performed to test whether or not ANT-1 binds to AR in living cells. A plasmid expressing Myc-tagged ANT-1 was transfected into COS-7 cells together with expression plasmid for the full-length or truncated mutants of AR, and then the cells were maintained with or without 10^{-8} M DHT. The full-length AR was specifically precipitated with Myc-tagged ANT-1 in the presence of DHT (Fig. 3, *a* and *b*). In addition, AR-AF-1, which exists in the nucleus without DHT (44), was precipitated with Myc-tagged ANT-1 in a ligand-independent fashion (Fig. 3*c*). In contrast to the *in vitro* binding in the GST

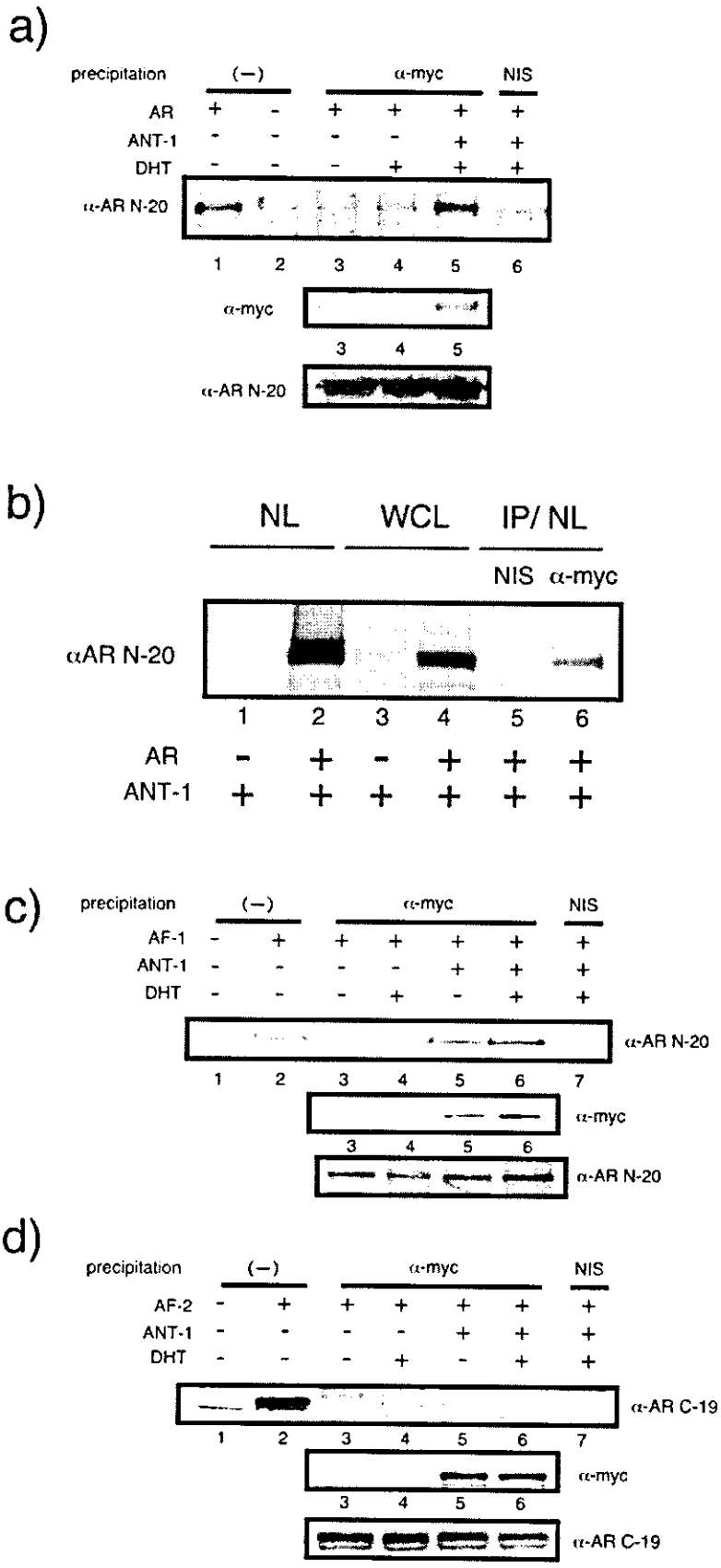

FIG. 3. **Immunocoprecipitation of ANT-1 with the full-length AR, AR-AF-1, or AR- AF-2.** The immunoprecipitation was performed using an antibody against Myc, and the precipitate was subjected to a Western blot analysis using the antibody N-20 for the full-length or AR-AF-1 and the antibody C-19 for the AR-AF-2. In each panel, the *middle* and the *bottom blot* represent the Western blot findings of the lysates used for the immunocoprecipitation, as controls. *a*, immunocoprecipitation of the full-length AR. For the immunocoprecipitation using non-immune normal rabbit serum for *lane 6*, the lysates for the precipitation was the same as those used for *lane 5*. *NIS*, non-immune normal rabbit serum. *b*, immunocoprecipitation using nuclear lysates. The cells were treated with 10^{-8} M DHT, and the nuclear lysates were prepared previously as described (39). *Lanes 1–4* are nuclear (*NL*) or whole cell (*WCL*) lysates before the immunocoprecipitation. For the immunocoprecipitation using nuclear lysates (*IP/NL*), the lysates were the same as those used for *lane 2*. *c*, immunocoprecipitation of AR-AF-1 with the Myc-tagged ANT-1. For *lanes 6* and *7*, the same whole cell lysates were used. *d*, immunocoprecipitation of AR-AF-2 with the Myc-tagged ANT-1. For *lanes 6* and *7*, the same whole cell lysates were used.

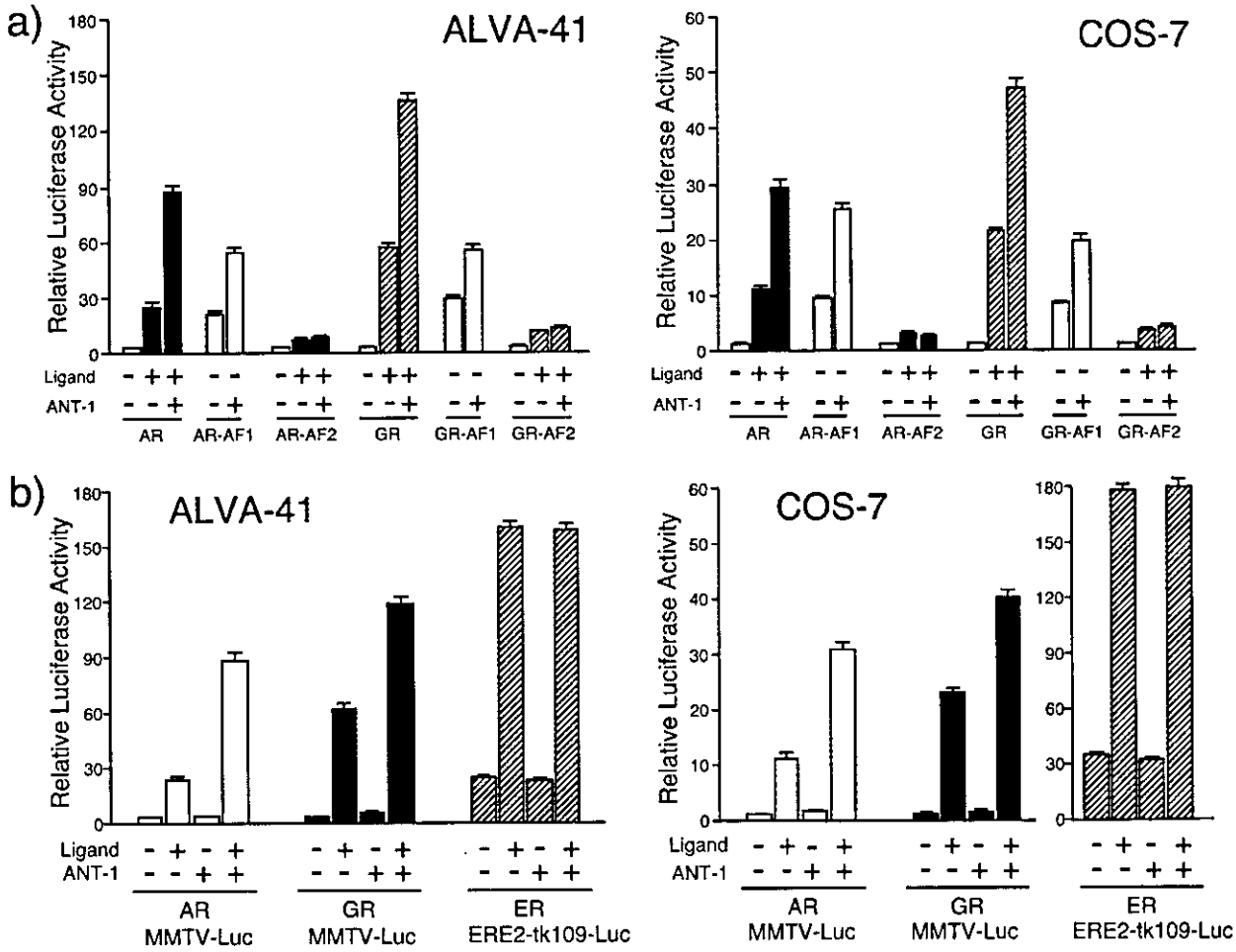

FIG. 4. **Functional analysis of ANT-1.** *a*, the ANT-1 enhances the AR-AF-1 or GR-AF-1 in a ligand-independent fashion. 1.0 μg of pMMTV-luc and the plasmids expressing the full-length or truncated AR or GR (0.2 μg) were transfected into ALVA-41 (*left*) or COS-7 cells (*right*) with or without 1.0 μg of pcDNA3-ANT, and the cells were treated with or without 10^{-8} M DHT or 10^{-7} M dexamethasone. *b*, the receptor specificity of ANT-1. The reporter plasmids and plasmids expressing ANT-1 were transfected into ALVA-41 or COS-7 cells with the cotransfection of the plasmids expressing full-length AR, GR, or ER, and then the transfected cells were treated with 10^{-8} M DHT, 10^{-7} M dexamethasone, and 10^{-8} M 17β-estradiol, respectively.

pull-down experiments, ANT-1 did not bind to AR-AF-2 in living cells (Fig. 3*d*).

ANT-1 Enhances AR- and GR-mediated but Not ER-mediated Transactivation Activities—To examine the effect of ANT-1 on the transactivation function of AR, GR, or ERα, we cotransfected an expression plasmid for each receptor together with the plasmids expressing ANT-1 and an appropriate reporter plasmid (pMMTV-luc for AR or GR, pERE2-tk109-luc for ERα, respectively) into ALVA-41 human prostatic cancer cells or COS-7 cells. The reporter gene *luc*+ (CLONTECH) harbored in pMMTV-luc does not contain any intronic sequences. As shown in Fig. 4*a*, ANT-1 further enhanced the ligand-induced transactivation function of full-length AR and GR (10^{-8} M DHT and 10^{-7} M dexamethasone, respectively). When the plasmid expressing the truncated AR-AF-1 (aa residues 1–622) or AR-AF-2 (aa residues 563–919) was transfected, ANT-1 enhanced the constitutive transactivation function mediated by AR-AF-1 by from 2- to 3-fold. However, no enhancement of the ligand-dependent transactivation mediated by AR-AF-2 was observed. A similar profile of the domain-specific transactivation was also observed for GR. In contrast, ANT-1 did not enhance the ERα-dependent transactivation (Fig. 4*b*). Whereas the ANT-1 is identical to the human homologue (the p102 U5 snRNP-binding protein) of the yeast splicing factor prp6p, involved in the spliceosome (37, 45), the transfection of ANT-1 did not enhance the basal promoter activities of reporter plasmids measured by luciferase activity (data not shown). In addition, the reporter gene *luc*+ (pGL3-luc from CLONTECH) harbored in pMMTV-luc does not contain any intronic sequences. Therefore, it was suggested that the observed enhancements of the reporter gene activities were not mediated by the nonspecific enhancement of the splicing activities but were mediated through AR- or GR-dependent transcription. Together with the findings in the immunocoprecipitation experiments, we concluded that ANT-1 is primarily an AF-1 interacting transcriptional coactivator for AR or GR but not for ERα.

The ANT-1-mediated transactivation was further confirmed in a reporter assay using natural authentic promoter (P450 aromatase exon Ib upstream promoter (38)) transactivated by the endogenous GR in primary-cultured human skin fibroblast. In this experiment, the expression of ANT-1 further enhanced the GR-mediated aromatase gene promoter activities (Fig. 5*a*). Furthermore, ANT-1 exhibited an independent additive effect on the transactivation function of cyclin E (32) or SRC-1α (21), which is reported to interact with AR-AF-1 (Fig. 5*b*). When either ANT-1-truncated mutant covering the N-terminal half

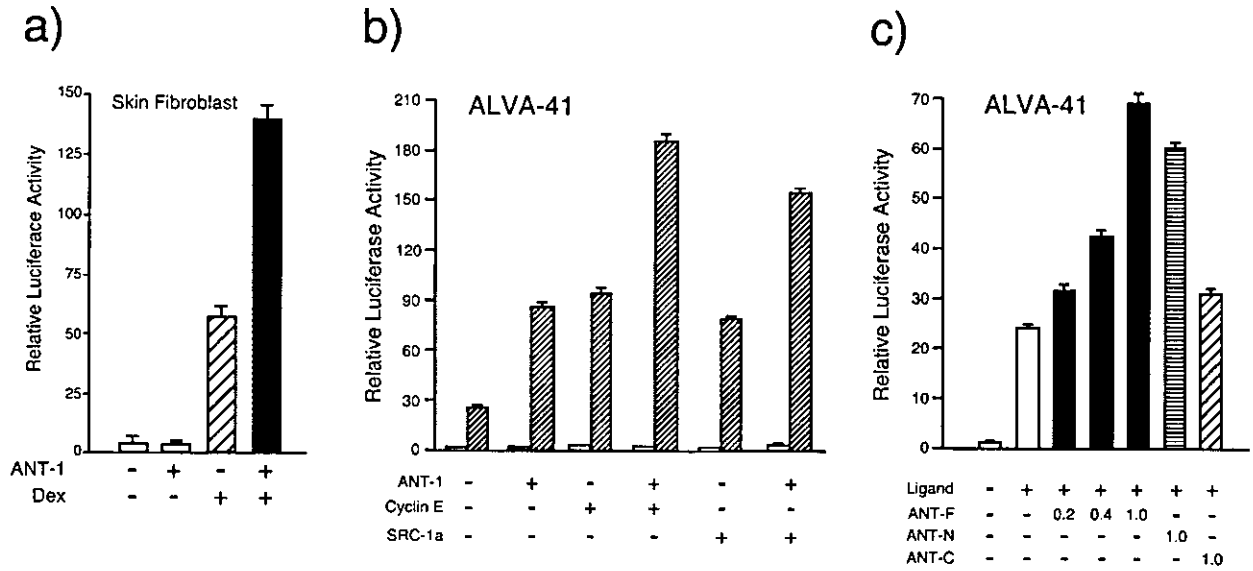

FIG. 5. *a*, the enhancement of the human aromatase exon Ib promoter activity. The reporter plasmid pAROM-luc driven by the human aromatase exon Ib promoter (−1101 to +60) was cotransfected into the primary-cultured human forearm skin fibroblasts with expression plasmids for ANT-1. 10^{-7} M dexamethasone was added to activate the gene by the endogenous GR binding to the glucocorticoid-response element located from −333 to −319 of the promoter Ib sequence. *b*, additive effects of ANT-1 with cyclin E or SRC-1a on the AR-dependent transactivation. The cells were transfected with the AR expression plasmid (0.2 μg) and also underwent the cotransfection of plasmids expressing 1.0 μg of ANT-1, cyclin E, SRC-1a, or the combination of the plasmids as shown. The total amount of the transfected DNA was kept constant (3.2 μg) by adding pcDNA3 empty vector plasmid. The cells were cultured with or without 10^{-8} M DHT (*dashed bar*, and *open bar*, respectively). *c*, the N-terminal 78–495-aa residues of ANT-1 is essential for the transactivating function of ANT-1. The two truncated mutants shown in Fig. 1*a* were used for the transfection experiments.

(78–495 aa), ANT (N), or ANT (C) covering the C-terminal half (495–941 aa) including one leucine zipper motif together with two LXXLL (Fig. 1*a*) motifs was expressed, ANT (N) alone enhanced the AR-mediated transactivation almost fully (90%) (Fig. 5*c*). This suggested that the transactivation domain(s) of ANT-1 exist within 78–495-aa residues.

Subcellular Localization of ANT-1—By using a high resolution three-dimensional reconstruction of the confocal microscopic images, we previously showed that transcriptionally active AR produces 250–400 small subnuclear speckles (Fig. 6*a*, applying a surface method (40)), which are shared with GR or ER. The liganded AR recruited the transcriptional cofactors such as SRC-1α, TIF-II, and p300/CBP into these subnuclear speckles (44). We were interested in the subnuclear spatial interrelation between nuclear receptor compartment, colocalizing with p160 members and p300/CBP, and splicing factor compartment. Therefore, the spatial interrelation of AR-CFP with ANT-1-YFP was explored in detail using a three-dimensional image analysis. A volume method in three-dimensional reconstruction showed the nuclear receptor speckles (fluorescence foci) and revealed many small spatial "pockets" where no cyan fluorescence was observed as in the nucleolus (Fig. 6*b*, *cyan* fluorescence was digitally converted into *red* as pseudocolor). The subnuclear localization of ANT-1 was clearly distinct from that of AR (Fig. 6*c*). In a good agreement with the subnuclear distribution of prp6p (yeast homologue of ANT-1) (45), the ANT-1 distribution was identical to the known distribution pattern of splicing factors (46–48). The transfected ANT-1-YFP distributed in the nucleus in two distinct patterns as follows: a diffuse fine reticular distribution throughout nucleus, devoid of a nucleolus, and a coarsely clustered distribution (speckles) known as the splicing factor compartment, both of which were exclusively in the euchromatin region where the Hoechst 33342 staining was less dense (Fig. 6*d*). When images of AR-CFP (Fig. 6*b*) and ANT-1-YFP (Fig. 6*c*) were spatially merged, the CFP and YFP fluorescence was colocalized only in the diffuse fine distribution (Fig. 6*e*, merged area is represented in *orange*). To focus on the spatial interrelation between ANT-1 speckles (splicing factor compartment) and AR-CFP (nuclear receptor speckles), the diffuse fine reticular distribution of ANT-1-YFP was cut off and expressed as a blank image (Fig. 6*f*). As a result, it became clear that the ANT-1 speckles fall into the small spatial pockets of the cyan fluorescence volume (Fig. 6, *b*, *g*, and *h*). When the image was digitally magnified (Fig. 6, *i–l*), the ANT-1 volume was shown to possess a rough surface, which was surrounded by a spatial mass representing transcriptionally active ARs without merging with each other (Fig. 6, *i* and *k*, surface views; Fig. 6, *j* and *l*, tomographic views).

DISCUSSION

By employing a swapped yeast two-hybrid system using AR-AF-1 as the bait, we identified a novel coactivator of AR-AF-1, named ANT-1. Functional reporter assays and the immunoprecipitation experiments demonstrated that the ANT-1 is essentially the AF-1-interacting transcriptional coactivator. The sequence of ANT-1 contains 19 TPR elements. The TPR motif consists of 34-amino acid residues containing the 8 loosely conserved sequence: WLGYAFAP (43). So far, more than 25 proteins possessing the TPR motif have been identified, and we have been shown to play important roles in the diverse biological functions, including transcriptional repression (49), a phosphorylation of nucleoproteins (50), and pre-mRNA splicing (51). The results shown in Fig. 5*c* suggest that the first 6 TPR motifs alone and/or upstream N-terminal sequence play a fundamental role in the ANT-1 function.

Whereas most of the transcriptional cofactors so far reported are known to interact with AF-2, the number of transcriptional cofactors specifically interacting with the AR-AF-1 sequence is limited. Interestingly, molecules that have been shown to bind to AR-AF-1 are apparently unique. They include SRA, ARA24 (12), ARA160 (16), BRCA1 (30), cdk-activating kinase (28),

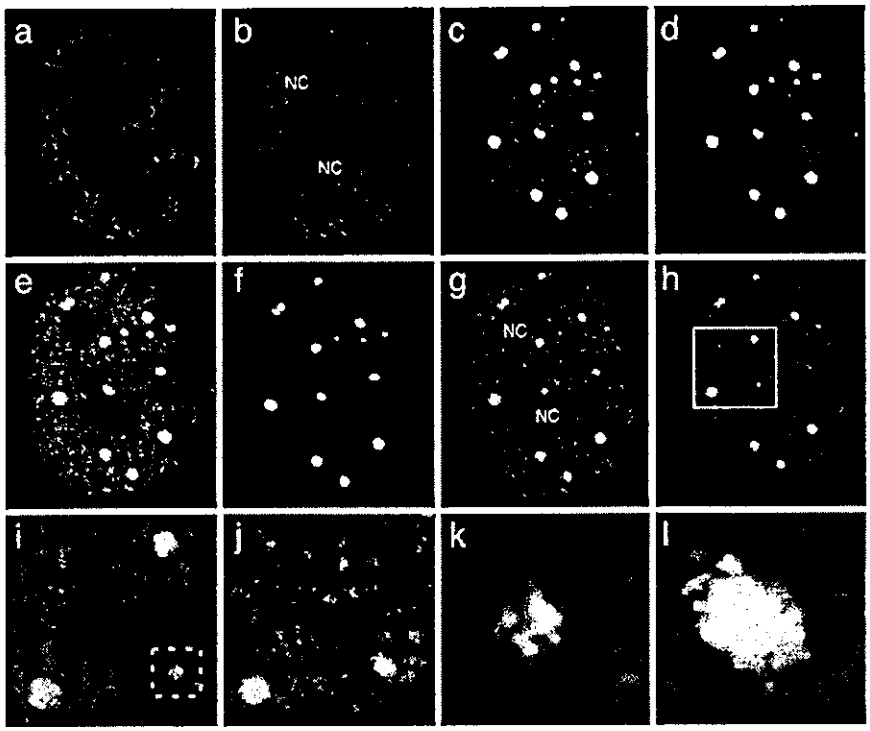

FIG. 6. **A three-dimensional analysis of the subnuclear compartmentalization of AR and ANT-1.** COS-7 cells were transfected with plasmids expressing AR-CFP fusion, ANT-1-YFP fusion, or both, treated with 10^{-8} M DHT, and then were stained with Hoechst 33342 (2 μg/ml) to visualize the chromatin structures (*blue*). A three-dimensional reconstruction was performed as described previously (40) for *a*, whereas deconvolution methods (nearest neighbors) were applied for other images. The AR-CFP is visualized in *red* as pseudocolor for all panels. For the chromatin images, less densely stained areas (namely euchromatin region) were shown as blank images, and densely stained areas (heterochromatin region) were shown as *blue*. *a*, the surface view of spatial merge of AR-CFP with chromatin structures. *b*, the surface view of AR-CFP. Note that in addition to the two nucleoli (*nc*), many small spatial pockets can be observed. *c*, the surface view of ANT-1-YFP compartments. *d*, the surface view of spatial merge of ANT-1-YFP with chromatin structures. *e*, the surface view of spatial merge of AR-CFP with ANT-1-YFP. *f*, the surface view of ANT-1-YFP compartments. To highlight the ANT-1 speckles, the diffusely distributed fine reticular network found in *c* was cut off and is shown as blank image. *g*, the surface view of the spatial merge of AR-CFP with ANT-1-YFP (*f*). The ANT-1 spatial mass falls into the several pockets found in *b*. *h*, the surface view of the spatial merge of AR-CFP, ANT-1-YFP, and chromatin images. *i*, the surface view of the spatial merge of AR-CFP, ANT-1-YFP, and chromatin images expressed in the volume method. The area indicated in the *white rectangle* in *h* is magnified in this view. *j*, the tomographic view of *i*. *k*, the magnified image highlighted with *dashed rectangle* in *i*. *l*, the tomographic view of *k*. The spatial mass representing the AR speckle does not merge with the YFP speckle, but instead it comes in contact with the YFP speckle at the periphery of the YFP speckle.

ART-27 (29), and cyclin E (32). For example, SRA (31) is an RNA molecule that has been shown to enhance the transactivation functions of the progesterone receptor, ER, GR, and AR by binding to AF-1. BRCA1, the mutation of which may play a role in the carcinogenesis of breast or ovary, also is thought to have implications regarding the proliferation of normal and malignant androgen-regulated tissues. In addition to these molecules, we presented evidence that ANT-1, p102 U5 snRNP-binding protein, binds to AR-AF-1. Together with the finding that cyclin E also interacts with U2 snRNP, AR-AF-1 may be involved in the spliceosomal machinery.

Transcripts synthesized by RNA polymerase II should undergo specific and extensive processing, including capping at the 5′ end, addition of the poly(A) tail, and the removal of the intervening sequences called splicing, before being transported into the cytoplasm. Especially in view of the splicing step, snRNPs play critical roles in composing the multiprotein-RNA complex called spliceosome. The splicing snRNPs (U1, U2, U4/U6, and U5) associate with pre-mRNA and with each other in an ordered sequence to form spliceosome, during which U5 snRNA base-pairs with exon sequences flanking the split sites. Furthermore, a component of U5 snRNP, called U5–200-kDa protein, which shares homologies with the DEAD box families of RNA helicases, was shown to unwind U4/U6 RNA duplexes (52). Interestingly, p72/68, a subfamily of the RNA helicase possessing DEAD box, functions as a novel class of ERα coactivator by enhancing the AF-1 transactivation capacity (39). It has been hypothesized that the active gene transcription simultaneously coupling with pre-mRNA processing may occur at the periphery of splicing factor compartment, and this process is called cotranscriptional splicing or "transcription-splicing coupling" (53–55). We presented further data supporting that transcription/splicing coupling may be evoked in a nuclear receptor-dependent fashion. This was first described in a peroxisome proliferator-activated receptor-γ-coactivator-1 (PGC-1), which possesses a pre-mRNA splicing activity itself (56). In AR, in addition to cyclin E-U2 snRNP interaction (33), FHL2, a tissue-specific AR cofactor (20), has been shown to interact with the polypyrimidine tract binding protein-associated splicing factor (57). However, FHL2 binds neither AR-AF-1 fragment nor AF-2 fragment alone but instead the full-length of the complete structure of AR is required for such binding. When the splicing activity of ANT-1 *per se* was assessed using an artificial luciferase minigene (kindly provided by Dr. S. Kato, University of Tokyo), we observed an increase in the minigene transcripts without enhancement of the splicing efficiency (data not shown). One possible explanation is that ANT-1 *per se* does not possess any splicing activity, but instead it functions as a transcriptional coactivator recruiting the active AR or GR into the active site of gene transcription coupled with mRNA splicing (54, 58). In this regard, it is shown that specific sets of proteins recruited as transcription coactivators function as

bridge proteins coupling the transcription factor and mRNA processing (59). However, further studies using the actual AR-target gene in place of the luciferase minigene still need to be performed.

In the nucleus, there exist different sets of functional compartments often called "foci" or "speckles," which include SFC that consists of nearly 20–50 large speckles (55), and nuclear receptor speckles possibly associated with the nuclear matrix structures (40, 44, 60–63). In contrast to the cytoplasmic compartments, the subnuclear compartments are not sequestered by the membrane structures, thus allowing the rapid movement of component proteins across the compartment. Splicing factor compartments consist of many protein complexes including snRNPs. We first visualized the spatial relationship between the steroid hormone receptor compartment and splicing factor compartment, thus revealing where the molecules locating in two distinct subnuclear compartments interact with each other. One is a nuclear receptor speckle, whereas another is the splicing factor compartment. We showed previously that the transcriptionally active ARs recruit chiefly AF-2-interacting transcriptional cofactors, such as TIF-II, with the functional interaction between AF-1 and AF-2, thus producing the fine subnuclear speckles in a p300/CBP-dependent fashion (44). In the three-dimensional image reconstruction, AR colocalized with ANT-1 only in diffusely distributed areas, whereas ANT-1 speckles representing splicing factor compartment were spatially distinct from but surrounded by the AR compartments. Recent studies (48, 64) have shown that the splicing factor compartment may represent the site for the storage and/or assembly of the splicing factors and that splicing factors can be rapidly recruited from the splicing factor compartment into the active sites of transcription. Furthermore, this high mobility is not restricted to the splicing factors but is a general feature of nuclear proteins, namely many nuclear proteins roam the cell nucleus in an energy-independent fashion (65). In this regard, the merging of the diffuse ANT-1 distribution with AR speckles near the splicing factor compartment may represent where the ANT-1 or ANT-1-snRNP complex meets the active AR-cofactor complex. The binding of ANT-1 with AR or GR might thus play a key role in the interaction between these two distinct sets of transcription factors located at distinct subnuclear compartments, namely the recruitment of transcriptionally active AR from the nuclear receptor compartment colocalizing with p160 and p300/CBP coactivators into the transcription-splicing coupling machinery formed near the periphery of the splicing factor compartment. Furthermore, ANT-1 may selectively recruit AR or GR, whereas ER, in which AF-1 transactivation is much weaker than that of AR or GR (23), is not recruited. Different sets of nuclear receptors, such as ER or peroxisome proliferator-activated receptor-γ, may therefore possess different compartment to compartment interaction mechanisms.

Acknowledgments—We thank Mitoshi Toki for assistance and excellent technical advice in creating the three-dimensional figures. We also thank Drs. Shigeaki Kato and Jun Yanagisawa for the kind gift of the plasmid construct and for useful discussions.

REFERENCES

1. Jenster, G., van der Korput, H. A., van Vroonhoven, C., van der Kwast, T. H., Trapman, J., and Brinkmann, A. O. (1991) *Mol. Endocrinol.* **5,** 1396–1404
2. Simental, J. A., Sar, M., Lane, M. V., French, F. S., and Wilson, E. M. (1991) *J. Biol. Chem.* **266,** 510–518
3. Beato, M., Chavez, S., and Truss, M. (1996) *Steroids* **61,** 240–251
4. Kalkhoven, E., Valentine, J. E., Heery, D. M., and Parker, M. G. (1998) *EMBO J.* **17,** 232–243
5. Kamei, Y., Xu, L., Heinzel, T., Torchia, J., Kurokawa, R., Gloss, B., Lin, S. C., Heyman, R. A., Rose, D. W., Glass, C. K., and Rosenfeld, M. G. (1996) *Cell* **85,** 403–414
6. Leers, J., Treuter, E., and Gustafsson, J. A. (1998) *Mol. Cell. Biol.* **18,** 6001–6013
7. Heinzel, T., Lavinsky, R. M., Mullen, T. M., Soderstrom, M., Laherty, C. D., Torchia, J., Yang, W. M., Brard, G., Ngo, S. D., Davie, J. R., Seto, E., Eisenman, R. N., Rose, D. W., Glass, C. K., and Rosenfeld, M. G. (1997) *Nature* **387,** 43–48
8. Ogryzko, V. V., Schiltz, R. L., Russanova, V., Howard, B. H., and Nakatani, Y. (1996) *Cell* **87,** 953–959
9. Ogryzko, V. V., Kotani, T., Zhang, X., Schiltz, R. L., Howard, T., Yang, X. J., Howard, B. H., Qin, J., and Nakatani, Y. (1998) *Cell* **94,** 35–44
10. Ito, M., Yuan, C. X., Malik, S., Gu, W., Fondell, J. D., Yamamura, S., Fu, Z. Y., Zhang, X., Qin, J., and Roeder, R. G. (1999) *Mol. Cell* **3,** 361–370
11. Sharma, M., Zarnegar, M., Li, X., Lim, B., and Sun, Z. (2000) *J. Biol. Chem.* **275,** 35200–35208
12. Hsiao, P. W., Lin, D. L., Nakao, R., and Chang, C. (1999) *J. Biol. Chem.* **274,** 20229–20234
13. Kang, H. Y., Yeh, S., Fujimoto, N., and Chang, C. (1999) *J. Biol. Chem.* **274,** 8570–8576
14. Fujimoto, N., Yeh, S., Kang, H. Y., Inui, S., Chang, H. C., Mizokami, A., and Chang, C. (1999) *J. Biol. Chem.* **274,** 8316–8321
15. Yeh, S., and Chang, C. (1996) *Proc. Natl. Acad. Sci. U. S. A.* **93,** 5517–5521
16. Hsiao, P. W., and Chang, C. (1999) *J. Biol. Chem.* **274,** 22373–22379
17. Yang, F., Li, X., Sharma, M., Zarnegar, M., Lim, B., and Sun, Z. (2001) *J. Biol. Chem.* **276,** 15345–15353
18. Lu, M. L., Schneider, M. C., Zheng, Y., Zhang, X., and Richie, J. P. (2001) *J. Biol. Chem.* **276,** 13442–13451
19. Brady, M. E., Ozanne, D. M., Gaughan, L., Waite, I., Cook, S., Neal, D. E., and Robson, C. N. (1999) *J. Biol. Chem.* **274,** 17599–17604
20. Muller, J. M., Isele, U., Metzger, E., Rempel, A., Moser, M., Pscherer, A., Breyer, T., Holubarsch, C., Buettner, R., and Schule, R. (2000) *EMBO J.* **19,** 359–369
21. Bevan, C. L., Hoare, S., Claessens, F., Heery, D. M., and Parker, M. G. (1999) *Mol. Cell. Biol.* **19,** 8383–8392
22. Alen, P., Claessens, F., Verhoeven, G., Rombauts, W., and Peeters, B. (1999) *Mol. Cell. Biol.* **19,** 6085–6097
23. Tora, L., White, J., Brou, C., Tasset, D., Webster, N., Scheer, E., and Chambon, P. (1989) *Cell* **59,** 477–487
24. Doesburg, P., Kuil, C. W., Berrevoets, C. A., Steketee, K., Faber, P. W., Mulder, E., Brinkmann, A. O., and Trapman, J. (1997) *Biochemistry* **36,** 1052–1064
25. Berrevoets, C. A., Doesburg, P., Steketee, K., Trapman, J., and Brinkmann, A. O. (1998) *Mol. Endocrinol.* **12,** 1172–1183
26. Quigley, C. A., De Bellis, A., Marschke, K. B., el-Awady, M. K., Wilson, E. M., and French, F. S. (1995) *Endocr. Rev.* **16,** 271–321
27. Tora, L., Gronemeyer, H., Turcotte, B., Gaub, M. P., and Chambon, P. (1988) *Nature* **333,** 185–188
28. Lee, D. K., Duan, H. O., and Chang, C. (2000) *J. Biol. Chem.* **275,** 9308–9313
29. Markus, S. M., Taneja, S. S., Logan, S. K., Li, W., Ha, S., Hittelman, A. B., Rogatsky, I., and Garabedian, M. J. (2002) *Mol. Biol. Cell* **13,** 670–682
30. Park, J. J., Irvine, R. A., Buchanan, G., Koh, S. S., Park, J. M., Tilley, W. D., Stallcup, M. R., Press, M. F., and Coetzee, G. A. (2000) *Cancer Res.* **60,** 5946–5949
31. Lanz, R. B., McKenna, N. J., Onate, S. A., Albrecht, U., Wong, J., Tsai, S. Y., Tsai, M. J., and O'Malley, B. W. (1999) *Cell* **97,** 17–27
32. Yamamoto, A., Hashimoto, Y., Kohri, K., Ogata, E., Kato, S., Ikeda, K., and Nakanishi, M. (2000) *J. Cell Biol.* **150,** 873–880
33. Seghezzi, W., Chua, K., Shanahan, F., Gozani, O., Reed, R., and Lees, E. (1998) *Mol. Cell. Biol.* **18,** 4526–4536
34. Adachi, M., Takayanagi, R., Tomura, A., Imasaki, K., Kato, S., Goto, K., Yanase, T., Ikuyama, S., and Nawata, H. (2000) *N. Engl. J. Med.* **343,** 856–862
35. Nishikimi, A., Mukai, J., Kioka, N., and Yamada, M. (1999) *Biochim. Biophys. Acta* **1435,** 147–152
36. Makarov, E. M., Makarova, O. V., Achsel, T., and Luhrmann, R. (2000) *J. Mol. Biol.* **298,** 567–575
37. Stevens, S. W., Ryan, D. E., Ge, H. Y., Moore, R. E., Young, M. K., Lee, T. D., and Abelson, J. (2002) *Mol. Cell* **9,** 31–44
38. Harada, N., Utsumi, T., and Takagi, Y. (1993) *Proc. Natl. Acad. Sci. U. S. A.* **90,** 11312–11316
39. Watanabe, M., Yanagisawa, J., Kitagawa, H., Takeyama, K., Ogawa, S., Arao, Y., Suzawa, M., Kobayashi, Y., Yano, T., Yoshikawa, H., Masuhiro, Y., and Kato, S. (2001) *EMBO J.* **20,** 1341–1352
40. Tomura, A., Goto, K., Morinaga, H., Nomura, M., Okabe, T., Yanase, T., Takayanagi, R., and Nawata, H. (2001) *J. Biol. Chem.* **276,** 28395–28401
41. Heery, D. M., Kalkhoven, E., Hoare, S., and Parker, M. G. (1997) *Nature* **387,** 733–736
42. Busch, S. J., and Sassone-Corsi, P. (1990) *Trends Genet.* **6,** 36–40
43. Goebl, M., and Yanagida, M. (1991) *Trends Biochem. Sci.* **16,** 173–177
44. Saito, M., Takayanagi, R., Goto, K., Fukamizu, A., Tomura, A., Yanase, T., and Nawata, H. (2002) *Mol. Endocrinol.* **16,** 694–706
45. Elliott, D. J., Bowman, D. S., Abovich, N., Fay, F. S., and Rosbash, M. (1992) *EMBO J.* **11,** 3731–3736
46. Spector, D. L. (1990) *Proc. Natl. Acad. Sci. U. S. A.* **87,** 147–151
47. Spector, D. L. (1993) *Curr. Opin. Cell Biol.* **5,** 442–447
48. Misteli, T., and Spector, D. L. (1998) *Curr. Opin. Cell Biol.* **10,** 323–331
49. Keleher, C. A., Redd, M. J., Schultz, J., Carlson, M., and Johnson, A. D. (1992) *Cell* **68,** 709–719
50. Chen, M. X., McPartlin, A. E., Brown, L., Chen, Y. H., Barker, H. M., and Cohen, P. T. (1994) *EMBO J.* **13,** 4278–4290
51. Legrain, P., and Choulika, A. (1990) *EMBO J.* **9,** 2775–2781
52. Laggerbauer, B., Achsel, T., and Luhrmann, R. (1998) *Proc. Natl. Acad. Sci. U. S. A.* **95,** 4188–4192
53. Xing, Y., Johnson, C. V., Moen, P. T., Jr., McNeil, J. A., and Lawrence, J. (1995) *J. Cell Biol.* **131,** 1635–1647
54. Misteli, T., and Spector, D. L. (1999) *Mol. Cell* **3,** 697–705
55. Misteli, T. (2000) *J. Cell Sci.* **113,** 1841–1849
56. Monsalve, M., Wu, Z., Adelmant, G., Puigserver, P., Fan, M., and Spiegelman,

B. M. (2000) *Mol. Cell* **6**, 307–316
57. Dye, B. T., and Patton, J. G. (2001) *Exp. Cell Res.* **263**, 131–144
58. Cramer, P., Srebrow, A., Kadener, S., Werbajh, S., de la Mata, M., Melen, G., Nogues, G., and Kornblihtt, A. R. (2001) *FEBS Lett.* **498**, 179–182
59. Ge, H., Si, Y., and Wolffe, A. P. (1998) *Mol. Cell* **2**, 751–759
60. Htun, H., Barsony, J., Renyi, I., Gould, D. L., and Hager, G. L. (1996) *Proc. Natl. Acad. Sci. U. S. A.* **93**, 4845–4850
61. Fejes-Toth, G., Pearce, D., and Naray-Fejes-Toth, A. (1998) *Proc. Natl. Acad. Sci. U. S. A.* **95**, 2973–2978
62. Htun, H., Holth, L. T., Walker, D., Davie, J. R., and Hager, G. L. (1999) *Mol. Biol. Cell* **10**, 471–486
63. Racz, A., and Barsony, J. (1999) *J. Biol. Chem.* **274**, 19352–19360
64. Misteli, T., Caceres, J. F., and Spector, D. L. (1997) *Nature* **387**, 523–527
65. Phair, R. D., and Misteli, T. (2000) *Nature* **404**, 604–609